

1 **Fluid Chemistry Evolution in Deep-Sea Hydrothermal Environments:**  
2 **Unraveling Mineral-Fluid-Microorganism Interactions through**  
3 **Continuous Culture Experiment**

4 Lise Artigue<sup>1\*</sup>, Valérie Chavagnac<sup>1</sup>, Christine Destrigneville<sup>1</sup>, David François<sup>2</sup>, Françoise  
5 Lesongeur<sup>2</sup>, Anne Godfroy<sup>2</sup>

6 <sup>1</sup> Géosciences Environnement Toulouse, GET, CNRS UMR 5563, UPS, IRD, Université de  
7 Toulouse, Toulouse, France

8 <sup>2</sup> Laboratoire de Biologie et d'Écologie des Écosystèmes marins Profonds, Ifremer, Univ Brest,  
9 CNRS, UMR 6197, Plouzané, France

10 **\* Correspondence:**

11 Lise Artigue

12 [artigue.get@gmail.com](mailto:artigue.get@gmail.com)

13 **Keywords:** Gaz-lift Bioreactor; Lithium isotopes; Strontium isotopes; Microbial diversity;  
14 Geochemical modeling; Lucky strike hydrothermal field

15  
16 **Highlights**

- 17 • Integrating Li/Sr isotopes tracers, microbial diversity and geochemical modeling.  
18 • Microbial diversity of the bioreactor fluid reflects the sulfate-based chimney one.  
19 • Microorganisms and minerals shape elemental and isotopic evolution in the fluid.  
20 • <sup>87</sup>Sr/<sup>86</sup>Sr ratio trace mineral-fluid-microorganism interactions, unlike  $\delta^7\text{Li}$ .

21  
22 **Abbreviations:**

23 LSHF, Lucky Strike Hydrothermal Field

24 Buoyant HF, Buoyant Hydrothermal Fluid

## 25 Abstract

26 This study investigates minerals and microorganisms effects on fluid chemistry through a  
27 continuous enrichment culture in a gas-lift bioreactor during the MoMARSat'19 cruise. A  
28 sulfate-based chimney and buoyant hydrothermal fluid, both collected *in situ* at the Aisics vent  
29 of the Lucky Strike hydrothermal field, were incubated for 18 days under physico-chemical  
30 conditions mimicking those of *in situ* diffuse vents. We present the evolution of elemental and  
31 Sr, and Li isotopic compositions of the bioreactor fluid, alongside Bacteria and Archaea  
32 diversity, and analyze the mineral saturation state of the fluid through geochemical modeling.  
33 Our results reveal that the microbial diversity in the bioreactor reflects that of the sulfate-based  
34 chimney. During the initial 168 h, minerals precipitation/dissolution primarily controlled the  
35 elemental and Sr isotopic composition of the fluid. From 168 h to 264 h, sulfate-reducing  
36 Archaea (*Archaeoglobi*) disappeared in favor of sulfur-reducing Archaea (*Thermoprotei* and  
37 *Thermococci*). This coincides with a drastic increase in trace element concentrations and less  
38 radiogenic  $^{87}\text{Sr}/^{86}\text{Sr}$  ratios, showcasing microbial influence on the fluid. From 264 h onwards,  
39 with stable sulfur-reducing archaeal diversity, mineral saturation state primarily controls the  
40 elemental composition of the fluid. However, we attribute the observed increase in the  $^{87}\text{Sr}/^{86}\text{Sr}$   
41 ratio and  $\delta^7\text{Li}$  to changes in bacterial diversity, notably increasing *Deinococci* abundance. This  
42 study reveals that in diffuse vent environments related to the sulfur cycle: (i) microorganism  
43 and mineral influence fluid chemistry over time, (ii) microbial diversity affects trace metal  
44 concentrations and isotopic signatures, and (iii) the  $^{87}\text{Sr}/^{86}\text{Sr}$  ratio trace mineral-fluid-  
45 microorganism interactions, unlike  $\delta^7\text{Li}$ .

## 46 1 Introduction

47 Hydrothermal vents are distributed along the 67,000 km long mid-ocean ridge system and have  
48 a global impact on ocean chemistry, particularly on trace elements and their isotopes (Elderfield  
49 & Schultz, 1996; German et al., 2016). These environments, characterized by chemical and  
50 physical gradients, offer habitats that support microorganisms growth, making them among the  
51 most biologically active regions in the deep ocean (Holden et al., 2012; Zeng et al., 2021). This  
52 biological activity involves interactions not only between organisms and chemical species but  
53 also between organisms and minerals (Breier et al., 2010; Edwards et al., 2005; Holden et al.,  
54 2012; Rogers et al., 2003). Despite significant progress in understanding hydrothermal  
55 biogeochemical processes, further research is crucial, particularly in unraveling the  
56 complexities of mineral-fluid-microorganism interactions and their influence on  
57 biogeochemical cycles (Holden et al., 2012).

58 To better comprehend water-rock interaction processes, lithium (Li) and strontium (Sr)  
59 concentrations and isotopes are widely used to trace geochemical processes notably in  
60 geothermal and hydrothermal systems (Araoka et al., 2016; Barker et al., 2008; Chavagnac,  
61 Leleu, et al., 2018; Millot et al., 2010; Wang et al., 2023). However, their complex oceanic  
62 budget remains unresolved (Davis et al., 2003; Teagle et al., 2003; Tomascak et al., 2016;  
63 Vance et al., 2009). Moreover, despite their bioaccumulation in marine organisms (Chowdhury  
64 & Blust, 2011; Thibon et al., 2021), few studies investigate the Sr and Li elements in relation  
65 to aquatic ecosystems (Burger & Lichtscheidl, 2019; Thibon et al., 2021; Thibon et al., 2023).  
66 It is essential to study the impact of Li and Sr on marine biota, especially considering the  
67 growing economic interest on these elements, which leads to studies on their extraction from  
68 seawater (Hong et al., 2018; Ryu et al., 2020; Vikström et al., 2013), particularly Li from black  
69 smokers hydrothermal vents, which contain 10–20 times more Li than seawater (Chavagnac,  
70 Leleu, et al., 2018; *European Commission, Study on the EU's List of Critical Raw Materials –*  
71 *Final Report*, 2020).

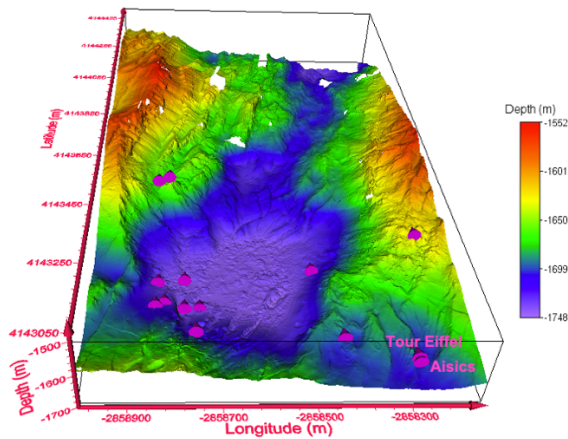
72 This study combines for the first time the elemental and Li and Sr isotopic tracers ( $\delta^7\text{Li}$ , and  
73  $^{87}\text{Sr}/^{86}\text{Sr}$  ratio) of the fluid with mineral saturation state obtained by thermodynamical modeling  
74 (PHREEQC), and microbial diversity analysis. This approach provides new insights into  
75 mineral-fluid-microorganism interactions. Studying microbial diversity at hydrothermal  
76 systems usually involves two approaches, the first one involves deploying *in situ* deep-sea  
77 devices (Alain et al., 2004; McCliment et al., 2006; Reysenbach et al., 2000; Rommevaux et  
78 al., 2019), while the second employs continuous enrichment culture in a laboratory. The second  
79 approach, used in this study, is the only one enabling the follow-up of microorganism  
80 interactions with dissolved chemical compounds and minerals overtime while controlling  
81 environmental conditions. Previous gas-lift bioreactor experiments were conducted to study  
82 deep-sea microbial communities evolution with constant fluid medium renewal (Callac et al.,  
83 2015; Godfroy et al., 2000; Godfroy et al., 2006; Postec, Pignet, et al., 2005; Postec et al., 2007;  
84 Raven et al., 1992). Only Callac et al (2015) collected both the inoculum and the culture  
85 medium *in situ* at a hydrothermal vent. In this study, we explore mineral-fluid-microorganism  
86 interactions through a continuous enrichment culture experiment conducted in a gas-lift  
87 bioreactor during the MoMARSat'19 cruise. Here, the inoculum is a portion of a hydrothermal  
88 chimney collected at the Aisics chimney at the foot step of the Tour Eiffel vent in the Lucky  
89 Strike Hydrothermal Field, and the culture medium is the Aisics' buoyant hydrothermal fluid,  
90 collected *in situ* between 100 and 150 °C. The sample is the top youngest part of the Aisics  
91 chimneys and is mainly composed of anhydrite. Anhydrite is commonly found in black  
92 smokers and impact marine biogeochemical cycle of calcium and sulfate. This study  
93 investigates the chemical evolution of the fluid once in contact with a sulfate-based chimney  
94 over an 18-day period, by analysing major and trace elements concentration, as well as lithium  
95 (Li) and strontium (Sr) isotopes, alongside mineralogy and microbial diversity. Furthermore,  
96 we discuss the impact of microorganisms on the Sr and Li concentrations and isotopic  
97 signatures of the fluid medium, unveiling new perspectives on the Li and Sr oceanic  
98 biogeochemical cycles.

## 99 **2 Materials and Methods**

### 100 **2.1 Study area**

101 The Lucky Strike Hydrothermal Field (LSHF) is located on the Mid-Atlantic Ridge at 37°17'N  
102 and 32°20'W, approximately 400 km to the Southwest of the Azores archipelago (Langmuir et  
103 al., 1997; Von Damm et al., 1998). This 1 km<sup>2</sup> hydrothermal vent field lies on a basaltic  
104 substratum and comprises 20 to 30 active vents distributed around a fossil lava lake (apart from  
105 Capelinhos vent) surrounded by three ancient volcanic cones (Charlou et al., 2000; Escartin et  
106 al., 2015; Fouquet et al., 1995; Langmuir et al., 1997; Ondréas et al., 2009; Von Damm et al.,  
107 1998). Fig. 1 presents the LSHF bathymetric map, at depths ranging between ~1550 and 1750  
108 m below sea level (mbsl), with 12 active hydrothermal sites. Of specific relevance for this study  
109 is the Aisics chimney, located southeast of the fossil lava lake, at the base of the Tour Eiffel  
110 hydrothermal edifice.

111



112

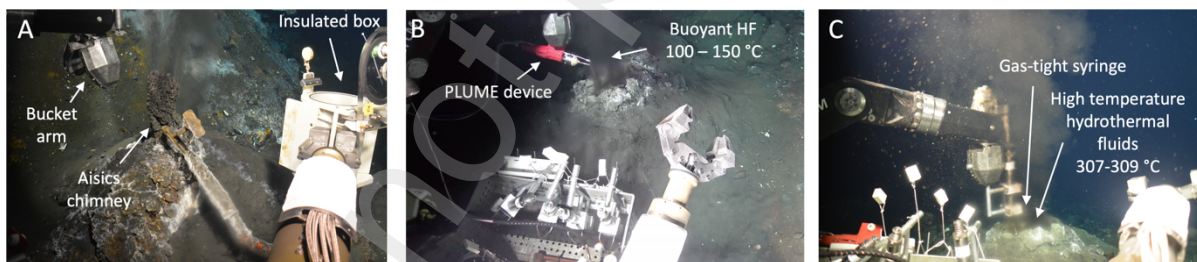
113 **Fig. 1** 3D bathymetric map of the Lucky Strike Hydrothermal Field (LSHF, Ondréas et al.,  
114 2009). Active vent locations are indicated by pink 3D cones.

115

## 116 2.2 Sample collection and onboard processing

117 During the MoMARsat'19 EMSO-Azores maintenance cruise aboard the *R.V. Pourquoi Pas?*  
118 (June - July 2019, Sarradin & Legrand, 2019), hydrothermal materials were collected at the  
119 LSHF using the hydraulic arm of the Human Operated Vehicle (HOV Nautile 6000).  
120 Successively, samples of hydrothermal chimney (Fig. 2a), buoyant hydrothermal fluid  
121 (buoyant HF, Fig. 2b), and high temperature hydrothermal fluid (end-members, Fig. 2c) were  
122 collected at the Aisics vent site. Upon recovery of the HOV Nautile on the research vessel, all  
123 samples were processed immediately in a shipboard chemical laboratory (Class 100 000, ISO  
124 8).

125



126

127

128 **Fig. 2** Chronological overview of scientific operations conducted at Aisics vent site. Snapshots  
129 of the HOV Nautile (Sarradin & Legrand, 2019) (A) Collection of Aisics' chimney sample  
130 using the bucket arm and an insulated box, (B) Sampling of the buoyant hydrothermal fluids  
131 (buoyant HF) with the PLUME device, and (C) Sampling of high-temperature hydrothermal  
132 fluids via gas-tight titanium syringe.

133

134 The anhydrite-bearing top of the Aisics chimney (sample number MOM19\_Aisics1, PL 1939-  
135 1, June 12<sup>th</sup> 2019) was collected using the bucket arm of the HOV Nautile and then dropped  
136 into a decontaminated insulated box (Fig. 2a). Before use, the insulated box was cleaned,  
137 disinfected with ethanol, and then filled with sterile distilled water (30 min, 121°C). To prevent  
138 atmospheric contamination before the dive and seawater contamination during the descent and  
139 ascent in the water column, the insulated box was opened and closed at depth upon chimney  
140 collection. Upon recovery of the HOV Nautile on the research vessel, the hydrothermal  
141 chimney was transferred into a sterile mortar under a laminar flow hood, and immediately

142 ground in a controlled anaerobic chamber under an N<sub>2</sub>/H<sub>2</sub> (90:10) atmosphere. The ground  
143 chimney was then stored in a glass flask until its introduction into the gas-lift bioreactor tank.  
144

145 The buoyant HF was collected unfiltered into 5L PVC/DEHP blood bags (Promepila, , sterilized  
146 by ethylene oxide) via the PLUME fluid pumping system implemented on the HOV Nautilé  
147 (Fig. 2b). Prior to each dive, the sampling tubes and cannulas of the PLUME device were rinsed  
148 with Milli-Q water, then filled with a small volume of Milli-Q water to prevent depression  
149 during descent. The temperature sensor, attached to the snorkel of the PLUME device, guided  
150 the HOV pilot in collecting the buoyant HF within the mixing gradient at temperature between  
151 100 and 150°C. All buoyant HF used in this study were collected at the Aisics vent at similar  
152 *in situ* temperatures during dives numbered 1939 on June 12<sup>th</sup> (2 blood bags; samples number  
153 MOM19\_PL1939-1\_PLUME3 and MOM19\_PL1939-1\_PLUME2), 1941 on June 14<sup>th</sup> (2  
154 blood bags, > 4L sample number MOM19\_PL1941-3\_PLUME2 and MOM19\_PL1941-  
155 3\_PLUME3), and 1955 on June 30<sup>th</sup> (1 blood bag, > 4L sample number MOM19 Aisics  
156 PL1955-17\_PLUME3). Upon recovery, each filled sterile blood bag was closed and stored at  
157 4 °C in a dark room prior to connection to the gas-lift bioreactor.

158 Prior to high temperature hydrothermal fluid sampling (Fig. 2c), the fluid temperature was  
159 measured *in situ* at 307 – 309 °C by inserting the HOV high temperature probe into the  
160 chimney. A total of eight high temperature hydrothermal fluid were sampled during two dives,  
161 on dive 1939 (June 12<sup>th</sup>, samples M19FLU01 to M19FLU04) and dive 1955 (June 30<sup>th</sup>, samples  
162 M19FLU49 to M19FLU52, Supplementary Material Table S1). These fluids were collected  
163 using 200 mL gas-tight titanium syringes. Prior to each dive, gas-tight titanium syringes were  
164 washed with diluted hydrochloric acid, then rinsed with ultrapure milli-Q water. The syringe  
165 snorkel was inserted into the chimney and operated individually by the hydraulic arm of the  
166 HOV Nautilé (Fig. 2c). Upon recovery, the high temperature hydrothermal fluids were  
167 extracted from gas-tight titanium syringes, filtered through 0.22 µm Millipore filters, split into  
168 distinct aliquots for onboard and onshore analysis, and stored at 4 °C in a dark room. Their  
169 chemical composition, analyzed using onshore instrumental and analytical facilities, allows the  
170 characterization of pure hydrothermal fluid end-member after extrapolation to Mg-zero prior  
171 to its dilution with the surrounding North Atlantic Deep Water (NADW).

172 For chemical analysis aboard the research vessel, pH, conductivity, salinity, Total Dissolved  
173 Solids (TDS), and redox potential (Eh) were measured immediately after fluid extraction using  
174 the Consort C562 multi-parameter analyzer. Total Sulfur (TS) and hydrogen sulfide (H<sub>2</sub>S)  
175 contents were measured with an amperometric micro-sensor (AquaMS, France), connected to  
176 both temperature and pH electrodes to establish equilibrium. Dissolved Fe (dFe) concentrations  
177 were measured with the HI96721 Iron High Range Photometer (range from 0 to 5 mg/L, Hanna  
178 instruments). The instrument was calibrated and validated using Hanna CAL CHECK™  
179 Standards. Prior to each day's measurements, the instrument was zeroed with a blank solution.  
180 The measurement accuracy is ± 0.04 mg/L ± 2% of reading.

181

### 182 **2.3 Gas-lift bioreactor**

183 A continuous enrichment culture experiment was conducted aboard the *R.V. Pourquoi Pas?*  
184 during the MoMARSat'19 cruise (Sarradin & Legrand, 2019), using a gas-lift bioreactor as  
185 shown on Fig. 3 (Callac et al., 2015; Godfroy et al., 2006; Postec, Urios, et al., 2005; Postec et  
186 al., 2007).

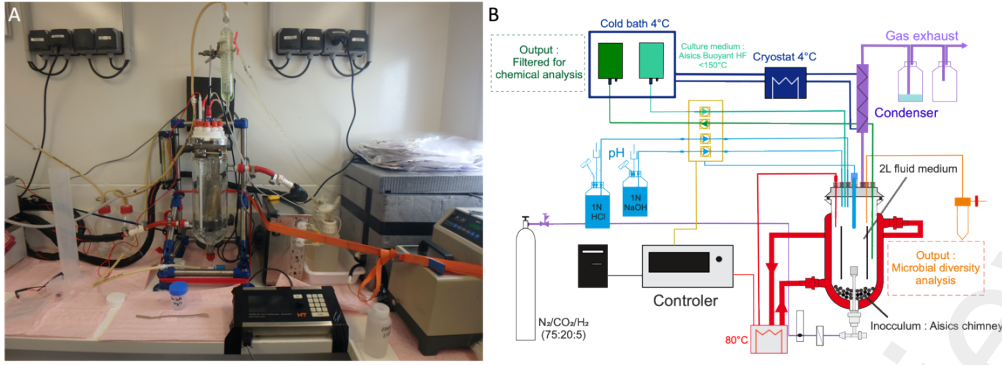


**Fig. 3** Set-up of the continuous enrichment culture experiment conducted aboard the *R.V. Pourquoi Pas?*. (A) Aboard photograph of the experiment in the laboratory. (B) Schematic illustration of the experimental setup, adapted from Godfroy et al (2006).

The aim of this experiment was to gain understanding on the chemical evolution of the fluid medium correlatively with hydrothermal microbial diversity and/or mineral precipitation/dissolution in a setting closely mimicking the *in situ* conditions of the diffuse hydrothermal environment.

The culture medium used in this study is the buoyant HF collected at the Aisics vent, with temperatures ranging between 100 and 150°C (see section 2.2). On June 13<sup>th</sup>, 2 L of the buoyant HF (sample MOM19\_PL1939-1\_PLUME3) were introduced into the gas-lift bioreactor tank. The conditions inside the bioreactor maintain a temperature of ~80 °C, a pressure of 1 atm, and anaerobic conditions thanks to a continuous gas flow of N<sub>2</sub>:CO<sub>2</sub>:H<sub>2</sub> (75:20:5 proportions, 10 cm<sup>3</sup>/minute flow rate). This continuous gas flow provides H<sub>2</sub> as the electron donor and CO<sub>2</sub> as the carbon source. During the experiment, the pH was controlled around 6.5 at 80°C (dead zone +/- 0.2) by adding either a 1 N HCl or 1N NaOH solution (Godfroy et al., 2006). After an hour and a half to reach incubation temperature and gas equilibrium, a sample of the culture medium (MOM19\_FERM\_T-1, Table 1) was filtered through a 0.22 μm Sterivex filter and split into different aliquots for subsequent aboard and onshore chemical analyses. Then, a 150 ml portion of the Aisics hydrothermal chimney (MOM19\_Aisics1, see section 2.2) was used as the inoculum and introduced into the bioreactor tank; this corresponds to the start of the experiment at T0. By then, we will use the term “fluid medium” to refer to the aqueous phase collected all along the experiment (samples labeled MOM19\_FERM\_T1 to T+18 for chemical analysis, Table 1, and MOM19.FerT0 to T18 for microbial analysis, Supplementary Material Table S2). The water/rock ratio is equal to 13 in the gas-lift bioreactor. The chimney was allowed to react with the buoyant HF for an 1 h 15 min before sampling for microbial diversity (MOM19.FerT0). Fifteen minutes after this sample, the continuous injection and withdrawal of fresh fluid began at a rate of 0.025 L/hour, maintaining a 2 L culture tank capacity. Throughout the 18-day/432-hour experiment, a total of four buoyant HF blood bags (collected on dives PL1939 and PL1941, see section 2.2) were used to maintain the capacity of the culture tank and were connected to the bioreactor at 0 h, 5 h, 120 h, and 288 h, respectively.

The mineralogical composition of the chimney sample was determined by X-Ray Diffraction analysis (XRD) both upon collection and at the end of the experiment. Upon collection, the inoculum was composed of 93 % of anhydrite (CaSO<sub>4</sub>), 3 % of pyrite (FeS<sub>2</sub>), 2 % halite (NaCl) and 1 % of chalcopyrite (CuFeS<sub>2</sub>). By the end of the experiment, the inoculum was composed of 91 % of anhydrite, 3 % of pyrite, 3 % halite, and 2 % of chalcopyrite (François, 2021).

226 During the course of the experiment it was not possible to sample the inoculum in the  
227 bioreactor.

228

229 For chemical analysis (notably elemental and isotope analysis), aliquots of (i) culture medium  
230 were extracted before inoculation (MOM19\_FERM\_T-1, Table 1), and (ii) fluid medium 24 h  
231 after the beginning of the experiment and then at 48-hour intervals over the following 18 days,  
232 resulting in a total of 10 additional samples (samples labeled MOM19\_FERM\_T1 to T18,  
233 Table 1). Each of these 10 samples corresponds to a 24h bioreactor withdrawal, and was  
234 collected in 600ml sterile Terumo blood bags, stored at 4°C (dark green output bags in Fig. 3B)  
235 and then filtered through 0.22 µm Sterivex filter prior to onboard and onshore chemical  
236 analyses.

237

238 For microbial diversity analysis (bacterial and archaeal diversity), both the chimney sample  
239 (sample MOM19\_Aisics1) and the buoyant HF fluid (sample M19PL1955\_PLUME3 filtered  
240 on Sterivex) were stored at - 80°C for subsequent onshore analysis. During the experiment, 50  
241 ml aliquots of the fluid medium were sampled daily (orange falcon on Fig. 3B) and stored at -  
242 80°C for microbial diversity analysis, resulting in a total of 19 samples (samples labeled  
243 MOM19.FerT0 to T18, Supplementary Material Table S2). Additionally, 1ml aliquots stored  
244 in a 9ml Sea water/2% formaldehyde solution and then were filtered through 0.22µm  
245 Nuclepore filters, stained with Sybr Gold for cell counting with an Axio Imager Z2 Apotome  
246 microscope (Carl Zeiss MicroImaging GmbH, Göttingen, Allemagne).

247

#### 248 **2.4 Microbial diversity analysis**

249 The microbial diversity analysis detailed below was conducted on the buoyant HF  
250 (M19PL1955 Plume 3 labeled 19.Ais.100.150 for molecular analysis), the chimney sample  
251 (MOM19\_Aisics1 labeled M19.Ais1 for molecular analysis), and on eighteen fluid medium  
252 samples (samples labeled MOM19.FerT0 to T18, Supplementary Material Table S2). A nested-  
253 PCR approach was used to amplify the variable regions V3-V4 of the archaeal 16S rRNA  
254 genes. The full-length archaeal 16S rDNA was amplified using the primers A24F-1492R  
255 (CGGTTGATCCTGCCGGA ; GGCTACCTTGTTACGACT, Lepage et al., 2004; Teske et  
256 al., 2002). The PCR products were gel purified and used as a template to amplify the V3-V4  
257 region by using the primers A344F-archaea806R (AYGGGGYGCASCAGGSG ;  
258 GGACTACVSGGGTATCTAAT, Stahl, 1991; Takai & Horikoshi, 2000). The archaeal 16S  
259 rRNA genes libraries were sequenced with Illumina MiSeq at MR DNA (Shallowater, TX,  
260 USA). The V3-V4 bacterial 16S rRNA genes libraries were prepared and sequenced with  
261 Illumina MiSeq at MR DNA (Shallowater, TX, USA) using the primers whoi341-who785R  
262 (CCTACGGGNGGCWGCAG ; GACTACHVGGGTATCTAATCC, Herlemann et al., 2011).  
263 The metabarcoding data were processed using the pipeline SAMBA  
264 (<https://github.com/ifremer-bioinformatics/samba>) which is based on QIIME 2 (Bolyen et al.,  
265 2019). Primers and barcode were removed using cutadapt (Martin, 2011), with the following  
266 parameters (errorRate = "0.1" ; overlap = "5"). Trimming of short reads and low quality  
267 sequences, ASVs inference and removal of chimeric sequences were performed using DADA2  
268 (Callahan et al., 2016) with the following parameters (FtrimLeft = "20" and RtrimLeft = "80"  
269 for *Archaea* ; FtrimLeft = "30" and RtrimLeft = "90" for *Bacteria* ; FmaxEE = "6" ; RmaxEE  
270 = "6" ; minQ = "3" ; chimeras = "consensus"). An additional step of ASV clustering has been  
271 performed using the dbOTU3 algorithm to avoid an overestimation of the diversity (Olesen et  
272 al., 2017). Taxonomic assignment of processed sequences was performed using the SILVA  
273 v138 reference database (Quast et al., 2012).

## 274 2.5 Elemental and isotopic analysis

275 All the chemical analyses were conducted at the Observatoire Midi-Pyrénées (Toulouse,  
276 France).

277 The analytical methods used for major dissolved cations (dCa, dK, dMg, dNa, dSi), anions  
278 (dCl, dBr, dSO<sub>4</sub>), and trace element (dBa, dFe, dMn, dLi, dSr) analyses are detailed in Besson  
279 et al (2014), Leleu (2017), Chavagnac et al (2018), and Artigue et al (2022) and will be briefly  
280 described below.

281 Bioreactor samples (samples labeled MOM19\_FERM\_T-1 to T18, Table 1) were diluted with  
282 Milli-Q water 30-fold for dCa, dK, dNa, and 10-fold for dMg and dSi concentration  
283 measurements. Other trace element concentrations were measured in pure solutions. All these  
284 element concentrations (except for dFe) were measured using an inductively coupled plasma  
285 atomic emission spectrometer (ICP-AES) Horiba Ultima2 instrument, with an analytical  
286 precision better than 2%. The ICP-AES was calibrated using mono elemental solution and an  
287 IAPSO seawater standard solution (OSIL Ltd. UK) diluted 10 to 200-fold with Milli-Q water.  
288 The analytical drift was quantified by the standard bracketing method every 8 samples.  
289 Detection limits were determined through daily repeated blank solutions (n = 10) at 0.2 µmol/L  
290 for dCa, 2 µmol/L for dK, 0.3 µmol/L for dMg, 20 µmol/L for dNa, 0.14 µmol/L for dSi, 0.01  
291 µmol/L for dBa, 0.02 µmol/L for dMn, 0.3 µmol/L for dLi, and 0.01 µmol/L for dSr.

292 Anion concentrations were measured in 10-fold diluted samples, and determined by anionic  
293 chromatography (Dionex ICS-2000) equipped with a specific column for a highly charged  
294 matrix (DIONEX IC AS19). The instrument was calibrated with IAPSO seawater standard  
295 diluted 10 to 50 folds with Milli-Q water. The instrument's error is 0.0001 ppm.

296 For isotopic measurements, all fluids were processed in a clean laboratory to isolate Li and Sr  
297 from their matrix using conventional liquid chromatography. For each element, 1 mL of  
298 individual fluid samples was evaporated to dryness in a Savillex beaker on a hot plate at 70 °C.  
299 The IAPSO and NASS 6 international standards were processed in the same manner and used  
300 alongside our samples.

301 Dissolved Sr was separated from the matrix using Sr-Spec resin (Eichrom, USA) following Pin  
302 et al (2014) protocol. Sr isotopic ratio (<sup>87</sup>Sr/<sup>86</sup>Sr) was measured using a Thermo Fisher Triton+  
303 Thermal Ionization Mass Spectrometer. The <sup>87</sup>Sr/<sup>86</sup>Sr ratio was defined as the average values  
304 of 150 measurements of ion intensities in the static multi-collection mode. The <sup>87</sup>Sr/<sup>86</sup>Sr ratios  
305 were corrected from mass fractionation using the <sup>86</sup>Sr/<sup>88</sup>Sr normalization ratio of 0.1194.  
306 Repeated measurements of the NBS 987 Sr standard gave a mean ratio of 0.710259 ± 0.000013  
307 (2 SD; n = 24; 2SE = 0.000003). The <sup>87</sup>Sr/<sup>86</sup>Sr ratios of our samples were corrected from the  
308 deviation of the measured NBS 987 to the recommended NBS 987 value of 0.710248.

309 The <sup>87</sup>Sr/<sup>86</sup>Sr ratios of international standards were measured to verify the accuracy of the  
310 measurements: 1. IAPSO seawater with a measured value of 0.709174 ± 0.000003 (2SD; n =  
311 4), consistent with published values of 0.709179 ± 0.000007 (2SD; n = 7; El Meknassi et al.,  
312 2020), and 2. NASS-6 seawater with a measured value of 0.709174 ± 0.000005 (2SD; n = 3),  
313 consistent with published values of 0.709179 ± 0.000014 (2SD; n = 8; Neymark et al., 2014).

314 Dissolved Li was separated from the NaCl-rich matrix using two steps ion exchange columns  
315 made of AGW-X12 200-400 mesh cation resin bed and eluted with 1N HCl (Protocol adapted  
316 to NaCl-solution from James & Palmer, 2000). The Li isotopic composition of each fluid  
317 sample was measured on a Thermo Fisher Triton+ Thermal Ionisation Mass Spectrometer at



318 the Observatoire Midi-Pyrénées. Additional information regarding sample loading and mass  
319 spectrometer setup can be found in Artigue et al (2022). The  $^7\text{Li}/^6\text{Li}$  ratios are expressed in the  
320  $\delta^7\text{Li}$  ‰ notation relative to the IRMM-16 Li standard ( $\text{Li}_2\text{CO}_3$ ) at similar Li concentration.  
321 Repeated measurements of the IRMM-16 standard gave a mean  $^7\text{Li}/^6\text{Li}$  ratio of  $12.082 \pm 0.012$   
322 (2SD;  $n = 17$ ), an internal precision of 0.25 ‰ (2SE) and an external precision of 1.03 ‰ (2SD;  
323  $n = 17$ ). The accuracy of our technique was verified against the measured ratios of the  
324 international IAPSO seawater standard with a measured value of  $+29.5 \pm 0.2$  ‰ (2SE),  
325 consistent with published values of  $+30.8 \pm 0.1$  ‰ (2SE, with external precision  $\leq 1\%$ , Rosner  
326 et al., 2007).

327

## 328 **2.6 Geochemical modeling**

329 Geochemical modeling was performed with the PHREEQC software package developed by  
330 USGS (Graphical User Interface Version 3, [www.usgs.gov/software/phreeqc-version-3](http://www.usgs.gov/software/phreeqc-version-3),  
331 Parkhurst & Appelo, 2013). PHREEQC can be used as a speciation program, particularly to  
332 calculate the distribution of aqueous species, and the possibility of mineral  
333 dissolution/precipitation. To perform these speciation calculations, PHREEQC requires the  
334 major elements total concentrations of the solution (user input) and the specific equilibrium  
335 constants from the PHREEQC databases. The saturation state of the fluid regarding to minerals  
336 is given by its saturation index (SI), which is calculated as the logarithm of the chemical  
337 activities of the dissolved ions (ion activity product, IAP) over their solubility constant (K).  
338 The possibility of a mineral to dissolve or precipitate is characterized by either undersaturation  
339 (SI < 0) or oversaturation (SI > 0).

340 In this study, the PHREEQC program was used along with the “lnl.dat” database (Johnson et  
341 al., 1992). This database provides logarithms of equilibrium constants (log K) along with  
342 thermodynamical data available up to 300 °C. The speciation modeling was run twice on the  
343 buoyant HF: first at its *in situ* temperature (126 °C), and then after reaching the incubation  
344 temperature (80 °C) and gas equilibrium of the gas-lift bioreactor. Subsequently, it was run on  
345 each aliquot of fluid medium extracted after inoculation from the gas-lift bioreactor (10  
346 samples, MOM19\_FERM\_T1 to T18). The chemical composition of the fluids was input as  
347 total concentrations of all previously analyzed chemical elements. To model the continuous  
348 gaseous flush of  $\text{N}_2:\text{CO}_2:\text{H}_2$ , thermodynamic equilibrium was established between the fluid and  
349 a gas phase at a total pressure of 1 atm and at the  $\text{N}_2:\text{CO}_2:\text{H}_2$  proportions (75:20:5) of the gas-  
350 lift bioreactor setup.

351 In the modeling, the oxidation potential was calculated regarding the  $\text{H}_2\text{S}/\text{SO}_4^{2-}$  redox couple.  
352 Li and Sr aqueous species distribution was calculated as well as the saturation indices (SI) for  
353 both the buoyant HF and the fluid medium throughout the entire duration of the bioreactor  
354 experiment.

### 355 3 Results

#### 356 3.1 Geochemistry of pure hydrothermal fluids

357 The geochemical features of the high temperature hydrothermal fluids collected during  
 358 MoMARSat'19 cruise are reported in Supplementary Material Table S1. High temperature  
 359 hydrothermal fluids exhibit pH values at 25 °C ranging between 3.58 and 4.40, and chemical  
 360 enrichment in dissolved Ca, K, Si, Fe, Mn, Si, and Li (dCa, dK, dSi, dFe, dMn, dLi) compared  
 361 to seawater. Since pure hydrothermal fluid should be totally dMg-depleted, the end-member  
 362 composition is obtained by linear extrapolation to zero-Mg of the least-square regression  
 363 method (Von Damm et al., 1998). The result is similar to previous end-member chemical  
 364 features obtained at this site (Chavagnac, Leleu, et al., 2018; Leleu, 2017). However, H<sub>2</sub>S  
 365 concentrations of 4.1 to 11.9 mmol/L, are much higher than previous values of 2 - 4 mmol/L  
 366 (Charlou et al., 2000; Chavagnac, Saleban Ali, et al., 2018; Pester et al., 2012; Von Damm et  
 367 al., 1998).

#### 369 3.2 Elemental and isotopic composition of bioreactor fluid medium

370 The elemental and isotopic composition of the buoyant HF, and all fluid medium extracted  
 371 from the gas-lift bioreactor are reported in Table 1 and are shown in Fig. 4.

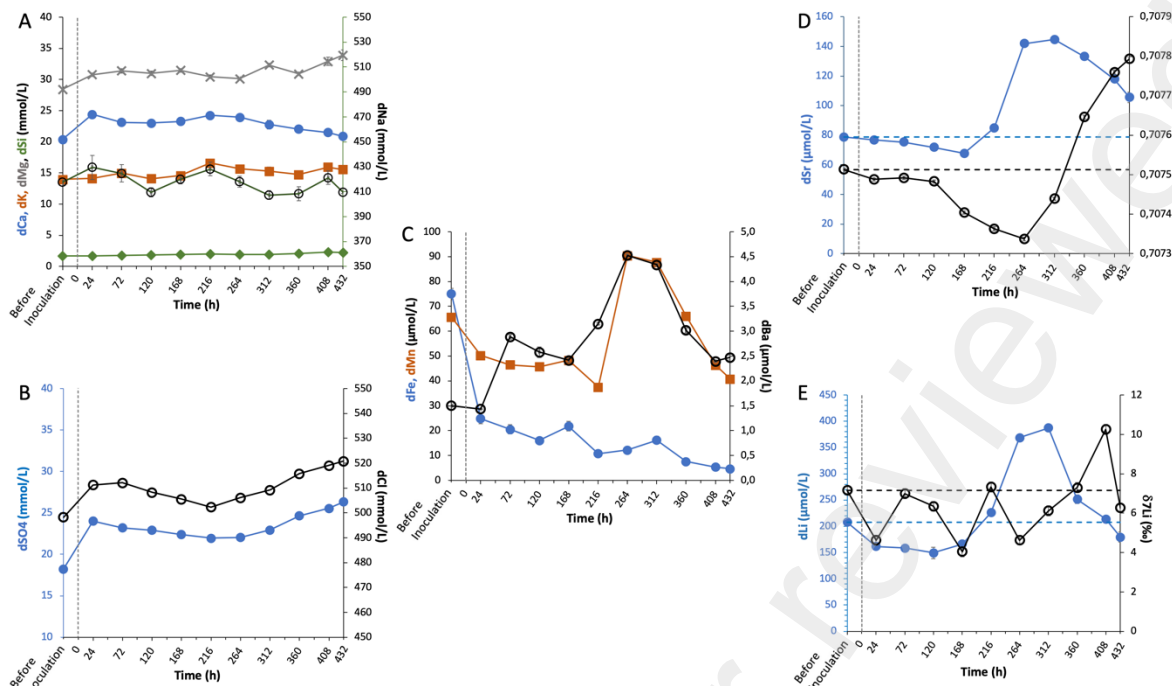
372

Buoyant HF (80 °C) MOM19_FERM_T-1 Before inoculation	Fluid medium (80 °C, sample labeled MOM19_FERM_T1 to T18)										
	T1 24 h	T3 72 h	T5 120 h	T7 168 h	T9 216 h	T11 264 h	T13 312 h	T15 360 h	T17 408 h	T18 432 h	
<b>Aboard analysis</b>											
pH	6.21	6.66	6.42	6.73	6.60	6.93	6.97	7.15	7.02	7.10	6.52
Total S (mg/L)	190	25	13	22.1	15	17	145	132	54	92	98
H <sub>2</sub> S (mmol/L)	1.0	0.6	0.1	0.5	0.2	0.4	0.2	1.3	0.8	1.1	1.8
Eh (mV)	3	-92	-18	118	-47	124	129	138	215	46	88
Conductivity (mS/cm)	43.5	46.6	47.3	46.7	46.4	45.1	45.9	44.6	47.1	47.2	47.2
TDS (g/L)	25.4	24.6	27.5	26.5	26.9	26.3	26.6	26	27.4	27.4	27.5
<b>Onshore analysis</b>											
dMg (mmol/L)	28.43	30.79	31.38	30.98	31.47	30.43	30.11	32.33	30.88	32.91	33.9
dCa (mmol/L)	20.37	24.39	23.12	23.01	23.28	24.23	23.94	22.78	22.03	21.5	20.88
dK (mmol/L)	13.97	14.12	14.96	14.1	14.57	16.59	15.65	15.27	14.75	15.94	15.55
dNa (mmol/L)	417.4	429.5	424.7	409.6	419.8	428.1	418	407.2	408.3	421.2	409.6
dFe (μmol/L)	75.1	24.8	20.5	16	21.8	10.8	12.2	16.2	7.6	5.4	4.7
dMn (μmol/L)	65.7	50.2	46.5	45.7	48.3	37.5	90.4	87.7	66.1	46.4	40.8
dSi (mmol/L)	1.68	1.67	1.76	1.82	1.93	1.96	1.94	1.92	2.1	2.32	2.22
dCl (mmol/L)	498.3	511.3	512.1	508.2	505.5	502.3	506.1	509.2	515.8	519.1	520.8
dSO <sub>4</sub> <sup>2-</sup> (mmol/L)	18.25	24.03	23.22	22.93	22.38	21.95	22.05	22.93	24.65	25.56	26.35
dBa (μmol/L)	1.5	1.4	2.9	2.6	2.4	3.1	4.5	4.3	3	2.4	2.5
dBr (μmol/L)	812	827	823	820	818	812	823	827	832	839	836
dSr (μmol/L)	79	77	75	72	68	85	142	145	133	118	106
<sup>87</sup> Sr/ <sup>86</sup> Sr	0.707513	0.707488	0.707492	0.707483	0.707404	0.707363	0.707337	0.707439	0.707646	0.707760	0.707794
± 2SE	± 0.000004	± 0.000004	± 0.000004	± 0.000004	± 0.000004	± 0.000005	± 0.000005	± 0.000004	± 0.000005	± 0.000005	± 0.000004
dLi (μmol/L)	208	162	158	149	166	226	369	387	251	214	179
δ <sup>7</sup> Li (‰)	7.2	4.6	7	6.3	4	7.3	4.6	6.1	7.3	10.3	6.3
<b>Ratios</b>											
dNa/dCl	0.84	0.84	0.83	0.81	0.83	0.85	0.83	0.8	0.79	0.81	0.79
dNa/dLi	2.01	2.66	2.68	2.74	2.52	1.89	1.13	1.05	1.62	1.97	2.28
dMg/dLi	0.14	0.19	0.20	0.21	0.19	0.13	0.08	0.08	0.12	0.15	0.19

373

374

375 **Table 1** Geochemical compositions in the gas-lift bioreactor of the buoyant hydrothermal  
 376 fluid (buoyant HF) before inoculation (MOM19\_FERM\_T-1), of the fluid medium 24h after  
 377 inoculation (MOM19\_FERM\_T1), and of fluid medium sampled at a 48-hour intervals until  
 378 the end of the experiment (MOM19\_FERM\_T3 to T18).



379  
380

381 **Fig. 4** Temporal evolution of the geochemical composition in the gas-lift bioreactor of the  
382 buoyant hydrothermal fluid (Buoyant HF) before inoculation, and of the fluid medium 24h  
383 after inoculation and at 48-hour intervals until the end of the experiment. The start of the  
384 experiment i.e. inoculation time is indicated at 0 h. (A) Major cation concentrations, (B) Major  
385 anion concentrations, (C) dFe, dMn, dBa concentrations, (D) dSr concentrations and  $^{87}\text{Sr}/^{86}\text{Sr}$   
386 ratios, and (E) dLi concentrations and  $\delta^7\text{Li}$  ‰ values. For (D) and (E), horizontal lines denote  
387 the initial values, aiding in visualizing fluctuations from the collection time to the end of the  
388 experiment. All data are plotted with their respective uncertainties.

389 The pH of the buoyant HF in the bioreactor before inoculation is 6.21. Throughout the  
390 experiment, pH values ranged between 6.42 and 7.15 (Table 1). Dissolved Na and dCl vary  
391 from 407 to 430 mmol/L and 502 to 521 mmol/L, respectively, and the dNa/dCl ratios show  
392 little variation at 0.79 – 0.85 compared to a standard seawater ratio of 0.86 (Millero et al.,  
393 2008). Between the sampling of the buoyant HF in the gas-lift bioreactor before inoculation  
394 (MOM19\_FERM\_T-1, Table 1) and the first sampling of the fluid medium for chemical  
395 analysis 24 hours after inoculation (MOM19\_FERM\_T1, Table 1), element concentrations  
396 exhibit various trends. Concentrations of dNa, dK, dCl, dBr, dBa, and dSr remain fairly  
397 constant, while dSO<sub>4</sub>, dCa, and dMg increase by up to 32%, 20%, and 8%, respectively.  
398 Conversely, concentrations of dFe, dMn, and dLi decrease by 67%, 24%, and 22%, respectively  
399 (Fig. 4). Then, from 24 h to 168h, element concentrations are overall constant, with slight  
400 reductions of dCa, dSO<sub>4</sub>, dMn, and dSr concentrations by up to 5%, 7%, 4%, and 12%,  
401 respectively (Fig. 4a, b, and d). Between 168 h and 264 h, major element concentrations remain  
402 stable; however, all trace element concentrations, except dFe, doubled (dMn, dBa, dSr, and  
403 dLi). Subsequently, from 264 h to the end of the experiment, trace elements, along with dCa,  
404 decreased progressively: dMn by 55%, dLi by 51%, dBa by 45%, dSr by 26%, and dCa by  
405 13%, while dSO<sub>4</sub> and dMg concentrations increased by up to 20% and 13%, respectively.  
406 Regarding the variability in dFe, it continuously decreases over time, by up to a factor of 5 by  
407 the end of the experiment (Fig. 4C).

408 The  $^{87}\text{Sr}/^{86}\text{Sr}$  ratio of the gas-lift bioreactor culture medium before inoculation was measured  
409 at  $0.707513 \pm 0.000004$  (MOM19\_FERM\_T-1, Table 1). From this sampling time to 24 h after  
410 the experiment start, the  $^{87}\text{Sr}/^{86}\text{Sr}$  ratio of the fluid medium decreases down to 0.707488,  
411 remaining relatively stable until 120 h, before decreasing to its minimum value of 0.707337 at  
412 264 h. From 264 h onwards, the  $^{87}\text{Sr}/^{86}\text{Sr}$  ratios continuously increase reaching a maximum  
413 value of 0.707794 by the end of the experiment (Fig. 4d). Regarding the Li isotopic  
414 composition, the  $\delta^7\text{Li}$  values show a large variation between +4.0 and +10.3 ‰ with a median  
415 value of +5.5 ‰ without any specific temporal evolution (Fig. 4e).

416

### 417 **3.4 PHREEQC geochemical modeling: saturation state and aqueous speciation**

418 PHREEQC geochemical modeling is controlled by the physico-chemical conditions of the  
419 experiment. It allows a thermodynamic diagnosis of the reactivity in the bioreactor fluid  
420 medium throughout the experiment, but doesn't account for kinetics. The mineral saturation  
421 indexes and element species abundances calculated by PHREEQC are presented in Table 2.  
422 Considering the observed minerals in the inoculum, thermodynamic calculations evidence the  
423 continuous undersaturation state of the medium fluid regarding anhydrite ( $\text{CaSO}_4$ ) throughout  
424 the experiment, suggesting anhydrite dissolution. However, the saturation indices of sulfides  
425 such as pyrite ( $\text{FeS}_2$ ) and chalcopyrite ( $\text{CuFeS}_2$ ), as well as oxides such as hematite ( $\text{Fe}_2\text{O}_3$ ),  
426 calcite ( $\text{CaCO}_3$ ) and other carbonates, and even barite ( $\text{BaSO}_4$ ) are all positive. This suggests  
427 either their stability in the fluid medium (for chalcopyrite) or their potential precipitation. Note  
428 that the continuous flushing of  $\text{N}_2:\text{CO}_2:\text{H}_2$  gaseous phase ensures anaerobic conditions which  
429 preserve sulfur mineralization.

430

431 Dissolved Sr speciation in solution is essentially composed of  $\text{Sr}^{2+}$ ,  $\text{SrCl}^+$  and  $\text{SrSO}_4$  species at  
432  $\sim 85\%$ ,  $\sim 10\%$  and  $\sim 4\%$ , respectively. The  $\text{SrCO}_3$  species is present at the percent level when  
433 pH of the fluid medium is close to 7 or above. Dissolved Li speciation consists of 98 % of  $\text{Li}^+$   
434 species with a contribution of  $\sim 1\%$  for  $\text{LiCl}$  and  $\text{LiSO}_4^-$  species.

435

	Buoyant HF (126 °C)	Buoyant HF (80 °C)	Fluid medium (80 °C, same labeled MOM19_FERM_T1 to T18)									
	MOM19-FERM T-1 <i>In situ</i>	MOM19-FERM T-1 Before inoculation	T1 24 h	T3 72 h	T5 120 h	T7 168 h	T9 216 h	T11 264 h	T13 312 h	T15 360 h	T17 408 h	T18 432 h
<b>Mineral saturation index (SI)</b>												
Anhydrite (CaSO <sub>4</sub> )	0.10	-0.30	-0.13	-0.17	-0.18	-0.18	-0.17	-0.19	-0.19	-0.18	-0.19	-0.16
Gypsum (CaSO <sub>4</sub> ·2H <sub>2</sub> O)	-0.58	-0.63	-0.46	-0.50	-0.51	-0.51	-0.50	-0.52	-0.52	-0.51	-0.53	-0.49
Barite (BaSO <sub>4</sub> )	-0.38	-0.02	0.06	0.35	0.31	0.26	0.37	0.54	0.53	0.42	0.32	0.34
Pyrite (FeS <sub>2</sub> )	8.15	9.57	7.58	7.00	7.31	7.10	6.94	8.55	8.65	7.60	7.81	7.88
Pyrrhotite (FeS)	3.18	2.79	1.50	1.17	1.49	1.18	1.13	2.33	2.35	1.68	1.81	1.30
Hematite (Fe <sub>2</sub> O <sub>3</sub> )	3.68	1.04	0.54	0.55	0.79	0.37	0.25	0.82	0.83	0.49	0.33	-1.22
Quartz (SiO <sub>2</sub> )	0.09	0.48	0.47	0.49	0.50	0.54	0.54	0.52	0.52	0.56	0.59	0.60
Strontianite (SrCO <sub>3</sub> )	-0.12	0.04	0.20	0.27	0.67	0.07	0.56	1.38	1.17	1.33	1.45	0.20
Calcite (CaCO <sub>3</sub> )	1.05	0.88	1.12	1.17	1.58	1.02	1.43	1.99	1.76	1.93	2.08	0.91
Rhodochrosite (MnCO <sub>3</sub> )	-0.20	0.03	0.07	0.12	0.53	-0.02	0.27	1.23	1.00	1.06	1.08	-0.16
<b>Species abundances (%)</b>												
<b>Lithium</b>												
Li <sup>+</sup>	98.0	98.2	98.0	98.0	98.0	98.1	98.1	98.1	98.0	97.9	97.9	97.9
LiCl	1.7	1.1	1.1	1.1	1.1	1.1	1.1	1.1	1.1	1.1	1.1	1.1
LiSO <sub>4</sub> <sup>-</sup>	0.4	0.7	0.9	0.9	0.9	0.8	0.8	0.9	0.9	1.0	1.0	1.0
LiOH	0.0	0.0	0.0	0.0	0.0	0.0	0.0	0.0	0.0	0.0	0.0	0.0
<b>Strontium</b>												
Sr <sup>2+</sup>	82.3	87.4	86.5	86.5	86.3	86.8	86.8	85.9	86.1	85.3	84.9	85.9
SrCl <sup>+</sup>	16.1	9.0	9.0	9.1	9.1	9.0	8.9	8.9	9.0	9.1	9.0	9.2
SrSO <sub>4</sub>	1.5	3.5	4.4	4.2	4.3	4.1	4.0	4.1	4.2	4.7	4.7	4.7
SrCO <sub>3</sub>	0.1	0.1	0.1	0.1	0.4	0.1	0.3	1.0	0.6	1.0	1.4	0.1
<b>Sulfide S(-II)</b>												
HS <sup>-</sup>	70.8	65.5	69.9	71.7	80.3	67.8	76.9	86.9	83.8	86.6	88.8	66.5
H <sub>2</sub> S	29.1	34.5	30.1	28.3	19.6	32.2	23.1	13.1	16.2	13.4	11.2	33.5
<b>Sulfate S(+VI)</b>												
MgSO <sub>4</sub>	58.5	37.3	36.6	37.4	37	38	36.6	35.3	37.7	35.6	36.1	39.0
SO <sub>4</sub> <sup>2-</sup>	26.1	39.0	38.9	38.6	39.3	38.2	38.8	40.2	39	40.7	40.3	38.3
NaSO <sub>4</sub> <sup>-</sup>	9.3	17.0	17.1	16.9	16.7	16.6	17.1	17.2	16.4	17.0	17.2	16.1
CaSO <sub>4</sub>	5.2	5.7	6.5	6.1	6.1	6.2	6.4	6.1	5.9	5.7	5.2	5.5
KSO <sub>4</sub> <sup>-</sup>	0.9	0.9	0.9	0.9	0.9	0.9	1.0	1.0	1.0	1.0	1.0	1.0

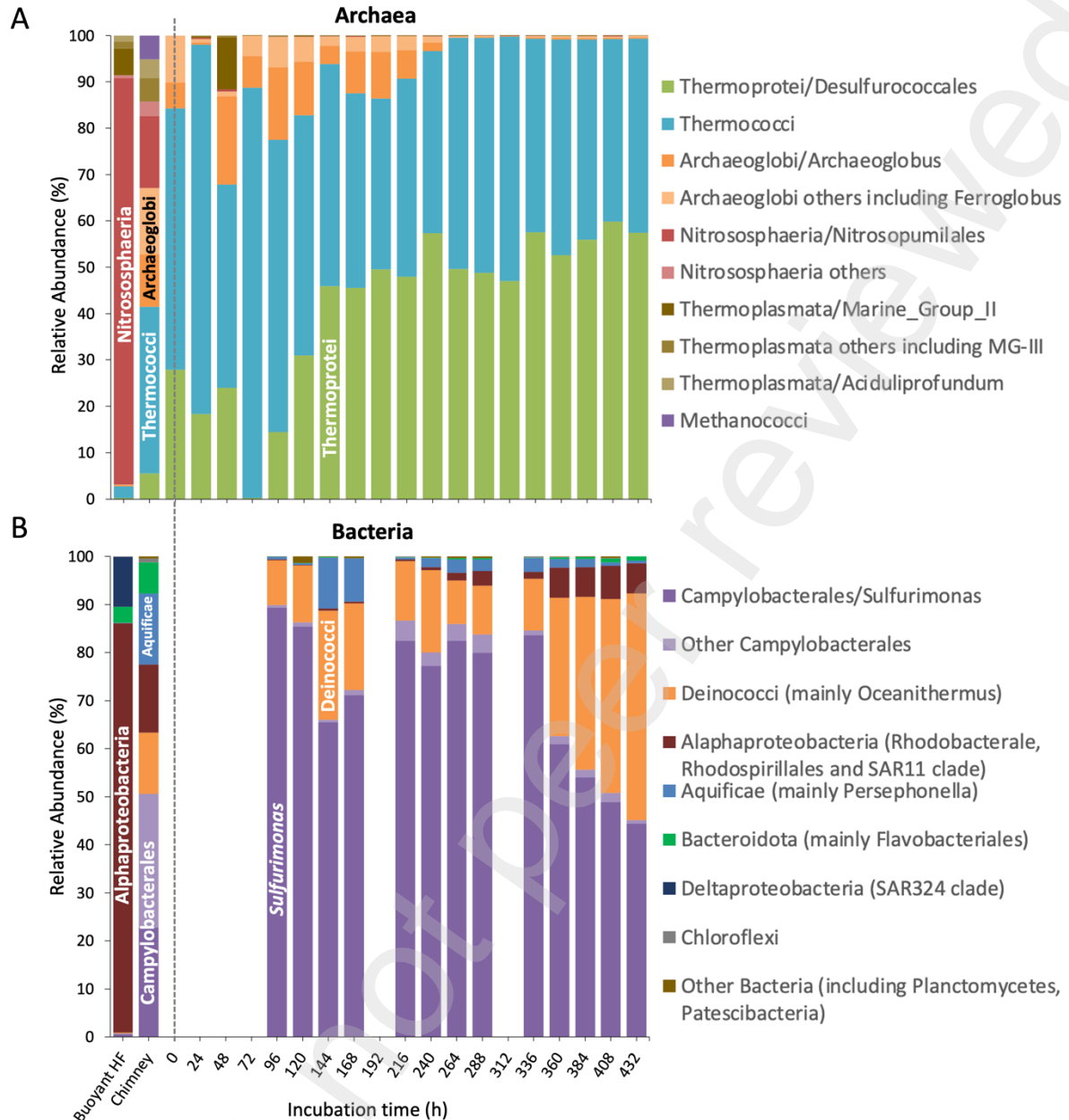
436  
437

438 **Table 2** Mineral saturation indexes and element species abundances of (i) the buoyant  
439 hydrothermal fluid (Buoyant HF) at *in situ* temperature (126 °C), (ii) the buoyant HF after  
440 reaching incubation temperature (80 °C) and gas equilibrium (MOM19\_FERM\_T-1), and (iii)  
441 the fluid medium 24 hours after inoculation (MOM19\_FERM\_T1), and then at 48 h intervals  
442 until the end of the experiment (MOM19\_FERM\_T3 to T18). All values were calculated using  
443 PHREEQC aqueous geochemical modeling.

444  
445  
446

### 3.5 Microbial diversity evolution in the bioreactor

447 The microbial diversity (bacterial and archaeal diversity) found throughout the experiment is  
448 presented in Fig. 5 and in Supplementary Material Table S2. These data show the relative  
449 abundance of the most representative taxa based on their sequence proportions. It is important  
450 to note that these data indicate the detected archaeal and bacterial taxa for each incubation time,  
451 thus conveying semi-quantitative variations.



452  
453

454 **Fig. 5** Barplots presenting the relative abundance of (A) Archaea and (B) Bacteria enriched in  
 455 the continuous culture over the incubation time (x-axis, hours). The microbial diversity in both  
 456 the Aisics chimney sample (used as the inoculum) and the buoyant hydrothermal fluid (buoyant  
 457 HF, used as the culture medium) is also presented. All taxa names are in the legend, with main  
 458 taxa labeled on corresponding bars for clarity.

459 The cell counts of microbial communities show an overall increase throughout the experiment,  
 460 reaching  $2 \times 10^5$  cell/mL at 120 h, then varying around  $6 \times 10^6$  cell/mL at 240 h before reaching  
 461 a maximum of  $8.5 \times 10^6$  cell/mL at 360 h, then cells concentration slightly decrease to reach  
 462  $4 \times 10^6$  cells/mL at the end of the experiment (François, 2021). At all sampling times, archaeal  
 463 sequences were detected, whereas no bacterial sequences were obtained until 96 hours, at 192  
 464 hours, and at 312 hours. This could be due to the sequencing reaction failing because of too  
 465 low bacterial abundance, or the number of sequences being too low once contaminants were

466 removed for bacterial diversity analysis. Due to the length of 16S RNA gene sequences  
467 obtained using illumina sequencing, identification of enriched microorganisms was possible  
468 up to the order level for Archaea and up to the genus level for some Bacteria.

469  
470 The archaeal diversity within the buoyant HF is mainly dominated by the class Nitrososphaeria  
471 (88%), with the *Nitrosopumulales* being the most represented order (Fig. 5a, Supplementary  
472 Material Table S2). Nitrososphaeria was also detected in the chimney sample but at  
473 significantly lower abundance (19%) compared to the buoyant HF. Within the chimney,  
474 Thermococci is the most abundant class (36%), followed by the Archaeoglobi class (26%)  
475 which includes *Archaeoglobus* and other genera such as *Ferroglobus*. Additionally, the class  
476 Thermoprotei, with the *Desulfurococcales* being its most represented order and the class  
477 Methanococci were detected in low abundance in the chimney (6% and 5%, respectively, Fig.  
478 5a). The class Thermoplasmata, including the genus *Aciduliprofundum* and Marine Group-III  
479 (MG-III), was detected at a few percent's in both buoyant HF and chimney samples (3% and  
480 9%, respectively), while the Thermoplasmata Marine Group-II (MG-II) was only detected in  
481 the buoyant HF (6%). Regarding bacterial diversity, the buoyant HF is largely dominated by  
482 the class Alphaproteobacteria (85%) including the orders *Rhodobacterales* and  
483 *Rhodospirillales*, and the SAR11 clade (Fig. 5b). Additionally, the class Deltaproteobacteria  
484 (SAR324 clade) and the Phylum Bacteroidota (mainly *Flavobacteriales* order) are also present  
485 in the buoyant HF, albeit at low (10%) and very low abundances (3%), respectively. By  
486 contrast, the chimney sample display higher bacterial diversity with the *Campylobacterales*  
487 order (including *Sulfurimonas* genus and other *Campylobacterales*) being dominant (51%), and  
488 classes such as Aquificae (mainly *Persephonella* genus), Deinococci (mainly *Oceanithermus*  
489 genus), Alphaproteobacteria, and Bacteroidota being detected at 15%, 13%, 14%, 6%,  
490 respectively. Throughout the 432 hours experiment, both archaeal and bacterial diversities of  
491 the fluid medium showed closer similarity to the chimney sample communities rather than to  
492 the buoyant HF ones. In the fluid medium, Thermococci and Themoprotei are the most  
493 abundant archaea classes, except at 72 h where no Thermoprotei were detected. Archaeoglobi  
494 represent between 3% and 22% of the Archaeal diversity during the first 240 hours (except at  
495 24h) but afterward decrease to less than 1% until the end of the experiment. Regarding bacterial  
496 diversity, the *Campylobacterales* genus *Sulfurimonas* dominates until 360 h (between 61% and  
497 89%), after which it shares prevalence with the Deinococci class (mainly *Oceanithermus*). Both  
498 Aquificae (mainly *Persephonella*) and Alphaproteobacteria classes were detected in almost all  
499 samples at very low abundance. However, Aquificae peaked at approximately 10% at 144 and  
500 168 hours and Alphaproteobacteria reached ~6% from 360 hours to the end of the experiment  
501 (Fig. 5b, Supplementary Material Table S2).

#### 502 503 **4. Discussion**

504 In the gas-lift bioreactor, the chemical and isotopic composition of the fluid medium results  
505 from interactions with minerals, microorganisms (archaea and bacteria) and gases (bioreactor  
506 setup conditions). In section 4.1, we will first characterize the collected materials, i.e., the  
507 Aisics chimney (used as the inoculum) and the buoyant HF (used as the culture medium), along  
508 with their microbial diversity. Once these materials are introduced into the gas-lift bioreactor,  
509 the experiment starts. In section 4.2, we will discuss how the elemental and isotopic chemical  
510 composition of the fluid medium respond to the evolution of microbial diversity and the mineral  
511 precipitation/dissolution processes.

512

#### 513 4.1 Characterization of the collected materials

514

515 The buoyant HF was collected *in situ* between 100 and 150°C (François, 2021). Both the  
516 buoyant HF and the end-member high temperature hydrothermal fluid exhibit enrichment in  
517 dCa, dK, dSi, dFe, dMn, dLi compared to seawater (Table 1 and S1, Leleu, 2017; Millero et  
518 al., 2008). The measured chemical composition of the buoyant HF can be modeled by an  
519 adiabatic and conservative mixing between Aisics hydrothermal end-member and NADW.  
520 Major cation and anion concentrations correspond to a contribution of 35 to 44 % of  
521 hydrothermal end member and a temperature range of 110 to 141 °C, consistent with the *in*-  
522 situ temperature of buoyant HF collection (100 – 150 °C, Supplementary Material Fig. S1).  
523 The buoyant HF is characterized by a  $^{87}\text{Sr}/^{86}\text{Sr}$  ratio of  $0.707513 \pm 0.000004$  and a  $\delta^7\text{Li}$  value  
524 of +7.2‰. While the Sr isotopic signature is fully coherent with those obtained through  
525 conservative mixing of 35 to 44% of the hydrothermal end-member with NADW, and the Li  
526 isotopic value corresponds to a 54% end-member contribution and a temperature of 170 °C  
527 (Supplementary Material Fig. S1). Contrarily to cations and anions, the end-member Sr and Li  
528 isotopic values were taken from AISICS end-member measurements between 2013 and 2015,  
529 as the 2019 values are not available (Artigue et al., 2022; Chavagnac, Leleu, et al., 2018; Leleu,  
530 2017). Thus, this discrepancy might be attributed to a slight change in the Aisics end-member  
531  $\delta^7\text{Li}$  value in 2019, or to potential fractionation processes during mixing between end-member  
532 and seawater. Indeed, while the instrument analysis of the  $^{87}\text{Sr}/^{86}\text{Sr}$  ratio eliminates mass-  
533 dependent Sr isotope fractionation occurring before or during the analysis (Andrews et al.,  
534 2016), the  $\delta^7\text{Li}$  values are affected by Li isotopes fractionation notably controlled by minerals  
535 precipitation/dissolution (Hindshaw et al., 2019; Vigier et al., 2008; Wang et al., 2023).

536

537 The inoculum is mainly composed of anhydrite (at 93%) which has a retrograde solubility at  
538 temperatures below 150 °C (Bischoff & Seyfried, 1978). Sulfur bearing minerals, pyrite and  
539 chalcopyrite, are present in smaller proportions (at 1 and 3%, respectively). These minerals can  
540 provide element and energy for sulfur or sulfate reducer or oxidizer microorganisms. Indeed,  
541 archaeal and bacterial development depends not only on the physico-chemical state of the  
542 buoyant HF or inoculum but also on the bioavailable energy sources provided through chemical  
543 components releasing and/or accepting electrons.

544

545 The microbial diversity (bacteria and archaea) is summarized in Supplementary Material Table  
546 S3, along with their origins in the gas-lift bioreactor (buoyant HF or chimney), their occurrence  
547 or absence in the fluid medium, optimal growth temperature, and main known metabolism.

548

549 The most abundant archaeal class found in the buoyant HF are Nistrosophaeria (mainly  
550 *Nitrosopumulales*), which are also present in the inoculum but at a lower abundance (Fig. 5a,  
551 Supplementary Material Table S2). Nistrosophaeria were already detected at hydrothermal  
552 environments (Takai et al., 2004; Teske et al., 2021) and commonly retrieved in deep sea water.  
553 At LSHF they were identified in microbial mats (associated or not with mussel assemblages)  
554 either located at the base of the Tour Eiffel vent at LSHF (< 10°C, Crépeau et al., 2011;  
555 Rommevaux et al., 2019) or at diffuse venting at the same site (40-55°C, Astorch-Cardona et  
556 al., 2023). However, Teske et al. (2021) suggest that Nistrosophaeria thrive is inhibited by  
557 acidic, anaerobic and high temperature conditions typical of such extreme environments.  
558 Indeed, this archaeal class finds ideal conditions of development in sea water environment  
559 characterized by aerobic, neutrophilic, and mesophilic conditions (Baker et al., 2012;  
560 Supplementary Material Table S3, Könneke et al., 2005; Qin et al., 2016; Qin et al., 2017). The  
561 class Thermoplasmata was also detected in the Buoyant HF, including the mesophilic marine  
562 groups MG-II and MG-III, as well as the thermoacidophilic genus *Aciduliprofundum*



563 (Supplementary Material Table S2, Reysenbach et al., 2006; Santoro et al., 2019). While  
564 *Aciduliprofundum* is commonly found in deep-sea vents, MG-II and MG-III are considered to  
565 be low in abundance in the deep sea and are rarely present in hydrothermal chimneys (François,  
566 2021; Haro-Moreno et al., 2017; Rinke et al., 2019; Zhang et al., 2015).

567 In the chimney sample, a few percent of *Aciduliprofundum* and MG-III, were also detected in  
568 the chimney but no MG-II. The most abundant archaeal classes in the chimney sample  
569 (inoculum) are Thermococci and Archaeoglobi, with Thermoprotei present to a lower extent  
570 (Fig. 5a and 6a). These taxa have been previously identified in deep-sea hydrothermal  
571 environments, notably at the Tour Eiffel site of the LSHF (Huber et al., 1997; Huber et al.,  
572 2006; Reysenbach et al., 2000; Rommevaux et al., 2019). These taxa have been described as  
573 anaerobes (or facultative anaerobes), (hyper)thermophilic, slightly acidophilic to alkaline  
574 (Supplementary Material Table S3 and reference therein). The Archaeoglobi class includes  
575 *Archaeoglobus* and other genera such as *Ferroglobus* (Fig. 5a, Supplementary Material Table  
576 S2). *Archaeoglobus* genus is able to reduce sulfate, sulfite, or thiosulfate compounds to H<sub>2</sub>S  
577 using organic substrate and/or H<sub>2</sub> as electron donors depending on the strain (dissimilatory  
578 sulfate reduction, Barton et al., 2014; Burggraf et al., 1990; Hartzell & Reed, 2006; Liu et al.,  
579 2012; Mori et al., 2008; Offre et al., 2013). *Ferroglobus* genus is known as an Fe(II) oxidizer  
580 or an Fe(III) reducer (Hafenbradl et al., 1996; Tor & Lovley, 2001). Both the Thermoprotei  
581 class, with *Desulfurococcales* as its most represented order, and the Thermococci class,  
582 including the *Thermococcales* order, have species involved in the sulfur cycle. Some  
583 *Desulfurococcales* can growth autotrophically by oxidizing hydrogen using sulfur, nitrate, or  
584 nitrite compounds as electron acceptor, and CO<sub>2</sub> as a carbon source. Organotrophic growth can  
585 also occur through aerobic respiration, anaerobic sulfur respiration with organic compounds as  
586 electron donors, or fermentation of organic compounds with elemental sulfur as the electron  
587 acceptor (Huber & Stetter, 2006; Liu et al., 2012). Note that some members of  
588 *Desulfurococcales* cannot use elemental sulfur or sulfur compounds (Huber & Stetter, 2006).  
589 *Thermococcales* species are organotrophic thermophiles that can also growth through  
590 fermentation of organic compounds with or without elemental sulfur (Bertoldo & Antranikian,  
591 2006; Liu et al., 2012). While elemental sulfur stimulates the growth of *Thermococcales*, it is  
592 not always essential, and some thrive without elemental sulfur. In the presence of elemental  
593 sulfur, it is reduced to H<sub>2</sub>S; in its absence, H<sub>2</sub> is produced by proton reduction (Schut et al.,  
594 2014). Some Methanococci were detected in the chimneys samples at a low abundance (5%).  
595 Methanococci are methanogenic archaea that produce methane from H<sub>2</sub> and CO<sub>2</sub>. While they  
596 are frequently detected at hydrothermal vents, they have not been previously found in Lucky  
597 Strike chimneys until now (Flores et al., 2011; Jeanthon et al., 1999; Jones et al., 1983; Jones  
598 et al., 1989; Whitman & Jeanthon, 2006).

599 The most abundant bacterial class identified in the buoyant HF is Alphaproteobacteria,  
600 including the orders *Rhodobacterales* and *Rhodospirillales*, and the SAR11 clade (Fig. 5B,  
601 Supplementary Material Table S2, Garrity et al., 2005). This class is also present to a lesser  
602 extent in the chimney sample, probably originating from the surrounding seawater. This class  
603 is described as ubiquitously distributed in the marine environment (Morris et al., 2002; Rappé  
604 et al., 2002) and notably found in black smoker chimneys (Voordeckers et al., 2008), microbial  
605 mats from the LSHF (Astorch-Cardona et al., 2023; Crépeau et al., 2011) and sediments  
606 (Cerqueira et al., 2017). SAR324, an uncultivated clade of Deltaproteobacteria, is only present  
607 in the buoyant HF (Fig. 5b, Fig. 6a). Known for its metabolic flexibility (Sheik et al., 2014;  
608 Swan et al., 2011; Wright et al., 1997), SAR324 clade can thrive in the full water column  
609 (Boeuf et al., 2021) and marine environments in the vicinity of hydrothermal sites (Dick et al.,  
610 2013; Dick & Tebo, 2010; François, 2021). Some Bacteroidota (mainly *Flavobacteriales*  
611 order) were detected at a few percents in both the buoyant HF and the chimney. Species of the  
612 *Flavobacteriales* order are primarily known to inhabit surface cold water environments

613 (Gómez-Pereira et al., 2010); however, one species was isolated from a biofilm on the surface  
614 of a black smoker chimney on the Arctic Mid-Ocean Ridge (Wissuwa et al., 2017). In the  
615 chimney sample, the bacterial abundance is dominated by *Campylobacteriales* with the  
616 *Sulfurimonas* genus, and other *Campylobacteriales*. Then, the rest of the bacterial diversity is  
617 shared between Alphaproteobacteria, Aquificae, Deinococci, and with a lower abundance  
618 Bacteroidota (mainly *Flavobacteriales*, Fig. 5b, Fig. 6a). All of these taxa have been previously  
619 found in deep-sea hydrothermal environments (Li et al., 2020; Miroshnichenko et al., 2003;  
620 Molari et al., 2023; Reysenbach et al., 2000; Sievert et al., 2000; Waite et al., 2017; Zeng et  
621 al., 2021; Zhang et al., 2016). *Sulfurimonas* and other *Campylobacteriales* and Aquificae  
622 (mainly *Persephonella*) were specifically identified at the LSHF and at the Aisics chimney of  
623 the Tour Eiffel site (François, 2021; François et al., 2021; Mino et al., 2017; Rommevaux et  
624 al., 2019). The *Sulfurimonas* genus is described as mesophilic chemolithoautotroph bacteria  
625 that grow at an optimum pH range from 4.5 to 8.6, relying on the presence of hydrogen,  
626 elemental sulfur or thiosulfate as the sole energy source, carbon dioxide as the sole carbon  
627 source, and ammonium or nitrate as the sole nitrogen source (François et al., 2021; Hu et al.,  
628 2021; Supplementary Material Table S3, Takai et al., 2006; Zeng et al., 2021). Bacteria from  
629 the Aquificae class (mainly *Persephonella*) are thermophilic and grow in microaerophilic  
630 conditions, oxidizing hydrogen, elemental sulfur, or thiosulfate using oxygen as an electron  
631 acceptor. In anaerobic conditions, they can also perform anaerobic nitrate reduction using  
632 hydrogen as electron donor and nitrate as electron acceptor ( François et al., 2021;  
633 Supplementary Material Table S3, Reysenbach et al., 2001; Zeng et al., 2021). A novel strain  
634 of the *Sulfurimonas* genus, designated as MO1340<sup>T</sup> and exhibiting similar metabolic properties  
635 to other *Persephonella* species, was isolated from the Aisics chimney (François, 2021; François  
636 et al., 2021). Deinococci (mainly *Vulcanithermus* genus) were detected in the chimney samples  
637 (Fig. 5b). *Vulcanithermus* genus grow between pH 5.5 and 8.4 and are capable of anaerobic  
638 growth by nitrate reduction, as well as lithoheterotrophic growth with molecular hydrogen  
639 (Supplementary Material Table S3, Miroshnichenko et al., 2003).  
640 The main archaeal and bacterial taxa identified in the collected buoyant HF and the chimney  
641 samples are illustrated in Fig. 6A, along with the mineral and chemical composition of the  
642 collected materials.

643

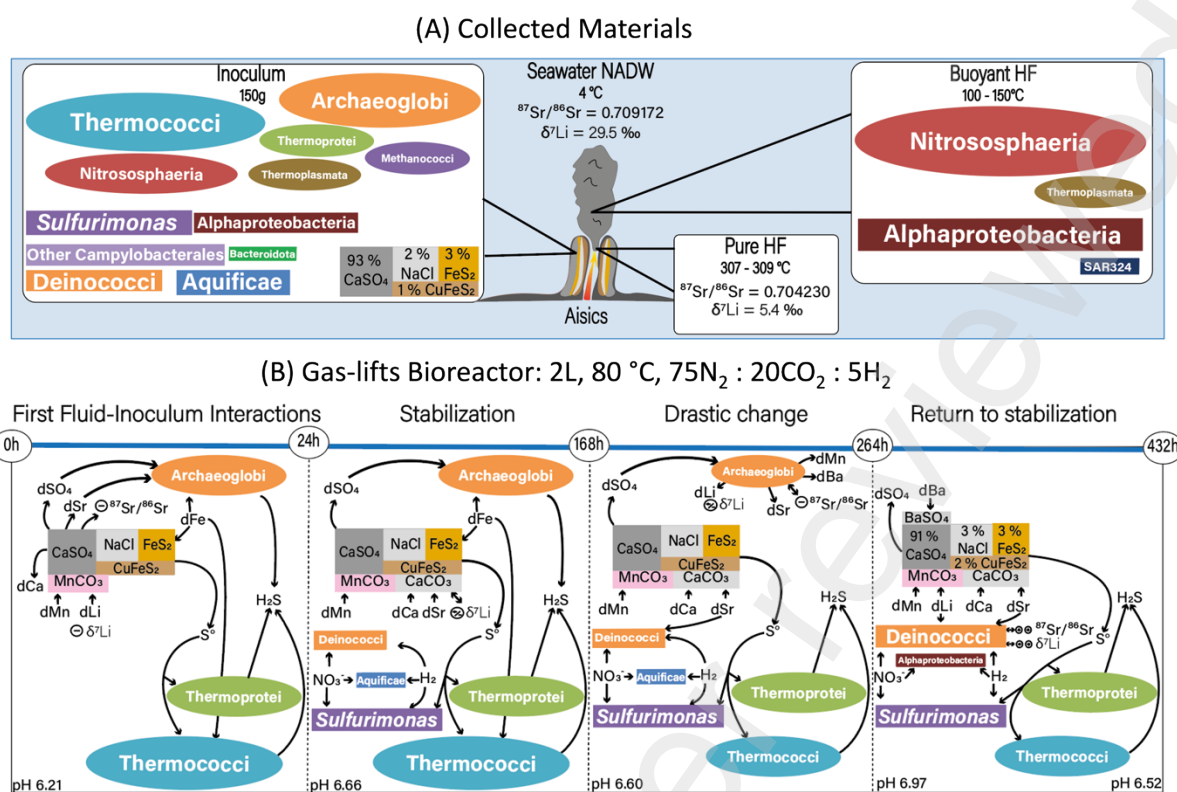
#### 644 **4.2 Elemental and isotopic evolution of the fluid medium: Impact of Mineral-fluid-** 645 **microorganism interactions**

646 Based on our results, we identify four time periods during which obvious and significant  
647 chemical variations are observed in trace element concentrations (except dFe) and Sr isotopic  
648 composition of the fluid medium. These four time intervals are: 1. First fluid-inoculum  
649 interactions (0 to 24 h), 2. Stabilization (24 to 168 h), 3. Drastic change (168 to 264 h), and 4.  
650 Return to stabilization (264 to 432 h, marking the end of the experiment). Note that the changes  
651 in blood bags throughout the experiment at 0 h, 5 h, 120 h, and 288 h (see section 2.3) are  
652 unrelated to the observed chemical, mineral, or microbial diversity changes. Fig. 6B is a  
653 schematic conceptual model illustrating the mineral-fluid-microorganism interactions  
654 occurring within the gas-lift bioreactor during these four-time intervals.

655

656

657



658  
659  
660  
661  
662  
663  
664  
665  
666  
667

**Fig. 6** Conceptual model illustrating (A) the mineral, microbial, and chemical composition of the collected materials: the high-temperature pure hydrothermal fluid (Pure HF), the buoyant hydrothermal fluid (Buoyant HF, culture medium), and the Aisics chimney (Inoculum). (B) The model showcases the impacts of mineral-fluid-microorganism interactions on the evolution of the fluid medium within the gas-lift bioreactor across four distinct time intervals: first fluid-inoculum interactions, stabilization, drastic change, and return to stabilization.

#### 4.2.1 First fluid-inoculum interactions: first 24 h

668 During this time interval, (i) the pH slightly increases from 6.21 to 6.66, (ii) the chemical  
669 concentrations in the fluid medium remain either constant ( $d\text{Na}$ ,  $d\text{K}$ ,  $d\text{Si}$ ,  $d\text{Cl}$ ,  $d\text{Br}$ , and  $d\text{Ba}$ ),  
670 increase ( $d\text{Ca}$ ,  $d\text{SO}_4$ , and  $d\text{Mg}$ ), or decrease ( $d\text{Fe}$ ,  $d\text{Mn}$ , and  $d\text{Li}$ ), (iii) the  $^{87}\text{Sr}/^{86}\text{Sr}$  ratio and  
671  $\delta^7\text{Li}$  value decrease, respectively, from 0.707513 and +7.2 ‰ in the buoyant HF down to  
672 0.707488 and +4.6 ‰ in the fluid medium at 24 h (Table 1, Fig. 4), and (iv) Nistrosphaeria  
673 class has disappeared in the gas-lift bioreactor, with sulfur-reducing archaea classes  
674 Thermoprotei and Thermococci prevailing over the sulfate-reducing archaea of the  
675 *Archaeoglobus* genus (Fig. 5a) and no bacteria were detected suggesting there are present at  
676 very low concentration (Fig. 5b).

677 Between the collection time of the buoyant HF and the beginning of the gaz-lift bioreactor  
678 experiment (0h), the temperature decreases from 126 °C to 80 °C, and the anhydrite saturation  
679 index shifts from being oversaturated ( $\text{SI} > 0$ ) to undersaturated ( $\text{SI} < 0$ , Table 2).  
680 Consequently, anhydrite can dissolve which can explain increasing  $d\text{Ca}$  and  $d\text{SO}_4$   
681 concentrations by up to 20 and 32%, respectively. Additionally, the increased  $d\text{SO}_4$   
682 concentration also change the  $d\text{Sr}$  and  $d\text{Li}$  speciation to higher  $\text{SrSO}_4$  and  $\text{LiSO}_4^-$   
683 concentrations (from 3.5 to 4.4% and 0.7 to 0.9%, respectively, Table 2). The  $d\text{Ca}$   
684 concentration increase of 4.02 mmol/L corresponds to the dissolution of 1.09 g of anhydrite,  
685 i.e., 0.8% of the inoculum. As the chimney sample was collected at immediate contact with  
686 high temperature hydrothermal fluid, we assume that the  $^{87}\text{Sr}/^{86}\text{Sr}$  ratio of anhydrite is similar

687 to that of the end-member hydrothermal fluid at the same site ( $0.704230 \pm 0.00004$ , Chavagnac,  
688 Leleu, et al., 2018; Leleu, 2017). Thus, its dissolution should induce a less radiogenic  $^{87}\text{Sr}/^{86}\text{Sr}$   
689 ratio in the fluid medium, as observed here.

690 Contrarily to anhydrite, pyrite and chalcopyrite as well as hematite remain oversaturated in the  
691 fluid medium ( $\text{SI} > 0$ ; Table 2), allowing their potential precipitation and the drastic decrease  
692 of dFe concentrations (- 67% of its initial concentration; Table 1, Fig. 4c).

693 Other trace metals such as dMn, and dLi also decrease in concentrations, by 24 and 22%,  
694 respectively (Fig. 4c, e). We attribute these variations to mineral precipitation, as the fluid  
695 medium is oversaturated ( $\text{SI} > 0$ ) regarding to carbonate minerals, notably rhodochrosite  
696 ( $\text{MnCO}_3$ ). The  $\delta^7\text{Li}$  value decreases as well from +7.2 to +4.6 ‰ in the fluid medium. Li isotope  
697 fractionation is known to be controlled by minerals precipitation/dissolution (Hindshaw et al.,  
698 2019; Vigier et al., 2008; Wang et al., 2023). Thus, even if the dLi concentration and  $\delta^7\text{Li}$  can  
699 be disrupted by adsorption on oxide surfaces (especially Mn-oxides, Chan & Hein, 2007), we  
700 cannot decipher here which minerals and processes can explain a lighter  $\delta^7\text{Li}$  signature. Li  
701 isotopes fractionation also depends on factors such as the temperature (Millot et al., 2010;  
702 Taylor et al., 2019), the water/rock ratio (Verney-Carron et al., 2015), the pH (Li & Liu, 2020),  
703 and  $\text{CO}_2$  concentrations in the solutions (Ji et al., 2022). However, all these factors are  
704 controlled and maintained in the bioreactor throughout the experiment.

705 The physico-chemical conditions in the gas-lift bioreactor (anaerobic environment maintained  
706 at 80 °C and pH ~6.5) are drastically unfavorable for the development of Nistrosphaeria,  
707 which are the most abundant archaea in the buoyant HF. They disappear from the fluid medium  
708 after 24 hours of incubation (Fig. 5a, Fig. 6b). In contrast, these conditions are favorable for  
709 the preservation and growth of Archaeoglobi, Thermococci, and Thermoprotei. It is noticeable  
710 that most enriched archaea that developed in the gas-lift bioreactor originated from the chimney  
711 sample (inoculum) rather than the buoyant HF, despite continuous feeding with fresh buoyant  
712 HF (Fig. 5a, Fig. 6b). With chemical features evidencing anhydrite dissolution, we anticipate  
713 that sulfate-reducing archaea such as *Archaeoglobus* would develop in such anaerobic  
714 conditions. However, *Archaeoglobus* and other Archaeoglobi are absent at 24 h which could  
715 be explained by their lowest growth rate compared to both Thermococci and Thermoprotei  
716 (Huber & Stetter, 2015a; Huber & Stetter, 2015b; Zillig & Reysenbach, 2015). The occurrence  
717 of Thermoprotei and Thermococci is coherent with the physico-chemical setup of the  
718 experiment. Indeed, both classes contain (hyper)thermophilic, anaerobic, and circumneutral  
719 species capable of organotrophic growth with or without elemental sulfur. Many  
720 *Thermococcales* grow better in the presence of elemental sulfur (see section 4.1, Huber &  
721 Stetter, 2006; Le Guellec et al., 2021; Liu et al., 2012). In the gas-lift bioreactor, elemental  
722 sulfur can be provided by sulfur-bearing minerals, i.e. pyrite and chalcopyrite, present in the  
723 chimney sample (Fig. 6).

724 The presence of genera such as *Ferroglobus* from the Archaeoglobi class and *Thermococcus*  
725 from the Thermococci class, known for their roles in iron metabolism, could also contribute to  
726 the observed significant decrease in dissolved iron (dFe). Indeed, *Thermococcus* reduces  
727 Fe(III), while *Ferroglobus* is capable of both oxidizing Fe(II) and reducing Fe(III) (Hafenbradl  
728 et al., 1996; Kashefi et al., 2002; Lim et al., 2020; Slobodkina et al., 2009; Tor & Lovley, 2001;  
729 Zeng et al., 2021).

#### 730 4.2.2 Stabilization: 24 h to 144 h

731 During this time interval, (i) the pH remains mainly stable around 6.6, (ii) the chemical  
732 concentrations in the fluid medium remain essentially constant, with slight reductions of dCa,  
733 dSO<sub>4</sub>, dMn, and dSr concentrations (Fig. 4a, b, and d), (iii) the <sup>87</sup>Sr/<sup>86</sup>Sr ratios remain stable at  
734 0.707488 ± 0.000005, contrary to the δ<sup>7</sup>Li value of the fluid medium, which fluctuates between  
735 +4.0 and +7.0 ‰ (Table 1, Fig. 4d and 4e), (iv) Thermococci are the most abundant archaea  
736 and Thermoprotei and Archaeoglobi are present, (v) only bacteria from the genus *Sulfurimonas*  
737 and Deinococci class are significantly abundant, with *Sulfurimonas* being the most prevalent  
738 (Fig. 6b).

739 The observed covariations of dCa, dSO<sub>4</sub> and dSr concentrations would suggest anhydrite  
740 (CaSO<sub>4</sub>) precipitation. However, the fluid medium is undersaturated regarding this mineral (SI  
741 < 0), precluding its precipitation (Table 2). Concomitant dCa and dSr concentrations decrease  
742 could be related to calcite precipitation (SI > 0, Table 2). In another gas-lift bioreactor study,  
743 Callac et al (2015) also observed a concomitant dCa and dSr concentrations evolution attributed  
744 to calcite - fluid medium interaction. The presence of calcite within the interstice of natural  
745 anhydrite chimney walls was already identified by Pagé et al (2008). Calcite precipitation  
746 induces Li isotope fractionation with a factor ranging from -8 to +2 ‰ depending on pH values  
747 and calcite growth rate (Füger et al., 2019; Füger et al., 2022; Marriott, Henderson, Belshaw,  
748 et al., 2004; Marriott, Henderson, Crompton, et al., 2004; Seyedali et al., 2021). This large  
749 range of fractionation factor could explain the δ<sup>7</sup>Li variability between +4.0 and +7.0 ‰.  
750 Moreover, the presence of *Archaeoglobus* genus of the Archaeoglobi class is coherent with  
751 calcite precipitation as they contribute to the total carbon mineralization process in marine  
752 sediments as sulfate reducing prokaryotes (Barton et al., 2014). Moreover, *Archaeoglobus* use  
753 dSO<sub>4</sub> in their metabolism which is coherent with the dSO<sub>4</sub> decrease observed here. Another  
754 carbonate mineral that can precipitate here is Rhodochrosite (SI > 0), whereby its precipitation  
755 could explain the observed decrease in dMn concentrations (Fig. 4C).

756  
757 Data on bacterial diversity in the fluid medium are available starting 96 hours after the start of  
758 the experiment (Fig. 5b). Among the bacteria identified in the buoyant HF and in the chimney  
759 sample (see section 4.1), only, *Sulfurimonas* genus from the *Campylobacterales* order and  
760 Deinococci class, are significantly abundant with *Sulfurimonas* largely dominating the  
761 diversity (Fig. 5b, Supplementary Material Table S2). As for the archaeal diversity, the most  
762 enriched bacteria thriving in the gas-lift bioreactor originates from the chimney sample rather  
763 than the buoyant HF. Mesophilic bacteria from *Sulfurimonas* genus was not expected to grow  
764 at such temperature (~ 80 °C) in the bioreactor (Supplementary Material Table S3).  
765 Nonetheless, *Sulfurimonas* genus was identified in various mesophilic and thermophilic  
766 hydrothermal habitats, including plumes, sediments, chimneys, and diffuse-flow fluids  
767 (Akerman et al., 2013; Hu et al., 2021; Inagaki, 2003; Li et al., 2020; Mino et al., 2017;  
768 Nakagawa et al., 2005). The presence of species at temperatures significantly above their  
769 known optimal growth temperature, such as *Sulfurimonas*, has previously been described in  
770 bioreactor enrichment culture experiments (Callac et al., 2015; Postec, Urios, et al., 2005).  
771 Aquificae, mainly *Persephonella* species, originating from the chimney sample, are initially  
772 detected at extremely low abundance (< 1%) in the fluid medium. However, their abundance  
773 increases to approximately 10% by 144 hours, comparable to that of the chimney sample  
774 (Supplementary Material Table S2, Fig. 5b). This is consistent with the known growth  
775 conditions of *Persephonella* species, which are suitable for our culture system (François et al.,  
776 2021). Here, the gas-lift bioreactor physico-chemical conditions (gas-flux composition and  
777 pyrite and chalcopyrite in the inoculum) provides all the essential growth prerequisites for  
778 Deinococci, and Aquificae.

#### 779 4.2.3 Drastic change: 168h to 264h

780 During this time interval, drastic changes are observed regarding trace element concentrations  
781 and their isotopes. Indeed, (i) the pH slightly increasing from 6.60 to 6.97; (ii) major element  
782 concentrations remain overall constant; (iii) all trace element concentrations (apart from dFe),  
783 drastically increase by a factor of two; (iv) the  $^{87}\text{Sr}/^{86}\text{Sr}$  ratio drastically decreases reaching a  
784 minimum value of 0.707337 at 264 h, while  $\delta^7\text{Li}$  values continue to fluctuate between +4.0 and  
785 7.3‰, (v) Archaeoglobi class progressively disappears; and (vi) the bacterial diversity (mainly  
786 *Sulfurimonas* and Deinococci) remains overall unchanged (Fig. 6b).

787

788 The mineral dissolution/precipitation does not explain the drastic trace elements increase.  
789 Indeed, the observed drastic increase of dMn, dLi, and dBa concentrations cannot be due to  
790 rhodochrosite and barite dissolution as the fluid medium is oversaturated regarding to both of  
791 them. The observed increase of dSr concentrations cannot be due to anhydrite dissolution even  
792 if anhydrite could dissolve (SI < 0), and supply dSr in the fluid medium. The increase of dSr  
793 concentrations by up to 74  $\mu\text{mol/L}$  would imply the dissolution of 9 g of anhydrite (assuming  
794 a Sr concentration  $\sim 1500$  ppm in anhydrite (Humphris & Bach, 2005), leading to a dCa and  
795 dSO<sub>4</sub> increase by up to 32 mmol/L, which is not observed here. Therefore, an effect of  
796 microbial diversity has to be addressed.

797 The bacterial diversity (mainly *Sulfurimonas* and Deinococci) and their relative abundance (66-  
798 82 % and 9-23%, respectively), remain overall constant. However, Archaeoglobi abundance  
799 seems to decrease over time, while sulfur-reducing archaea classes, i.e. Thermoprotei and  
800 Thermococci, are much more abundant, reaching both a relative abundance of 50% at 264 h.  
801 We observed that the progressive Archaeoglobi class low abundance is concomitant with an  
802 increase in dSr (as well as dMn, dLi, and dBa, Fig. 4) and less radiogenic  $^{87}\text{Sr}/^{86}\text{Sr}$  ratios from  
803 0.707483 down to 0.707337 in the fluid medium. We suggest that Archaeoglobi has the  
804 potential to store many trace metals via its metabolic pathway. Indeed, to sustain their  
805 metabolic demands, bacterial and archaeal cells have to ensure the supply of the right metals  
806 to the right proteins (Waldron & Robinson, 2009). This process, known as metal homeostasis,  
807 is based on the involvement of specific genes capable of sensing, transporting and storing any  
808 metals inside and between cells (Chandrangsu et al., 2017; Waldron & Robinson, 2009). Thus,  
809 it is possible that Archaeoglobi have stored dSr in their cells with other trace metals (dMn, dLi,  
810 and dBa), and progressively release them into the fluid medium when they vanish. Such process  
811 could lead to the observed less radiogenic  $^{87}\text{Sr}/^{86}\text{Sr}$  ratios from 0.707483 down to 0.707337.  
812 The  $\delta^7\text{Li}$  values fluctuates between +4.0 and +7.3 ‰ without any specific trend according to  
813 time. Poet et al (2023) showed that membrane transporters and channels transport  $^6\text{Li}$  faster  
814 than  $^7\text{Li}$ . Such process associated to Archaeoglobi should result in lower  $\delta^7\text{Li}$  one when they  
815 progressively disappear, which is not clearly evidenced here. Further studies on the link  
816 between Archaeoglobi class, trace metal storage and associated isotopic fractionation are  
817 therefore needed.

818

#### 819 4.2.4 Return to stabilization: 264 h to 432 h

820 We observed that (i) the pH remains stable at around 7 (ii) the chemical concentrations in the  
821 fluid medium either decrease (dCa, dMn, dBa, dSr, dLi), or increase (dSO<sub>4</sub>, and dMg), (iii)  
822 the  $^{87}\text{Sr}/^{86}\text{Sr}$  ratio and  $\delta^7\text{Li}$  values increases reaching a maximum of 0.707794 at 432 h and  
823 +10.3 ‰ at 408 h, respectively, (iv) the abundance of archaea classes remain stable and fully  
824 dominated by sulfur-reducing ones (Thermoprotei and Thermococci, each at 50%), (iv) the  
825 abundance of the Deinococci class increases, and significant abundance of Alphaproteobacteria  
826 is observed, while the relative abundance of *Sulfurimonas* decreases (Fig. 6b).

827 Contrarily to the previous time intervals, the observed decrease of dCa (-13%), dSr (-26%),  
828 dMn (-55%), dLi (-51%), and dBa (-45%) concentrations is coherent with calcite,  
829 rhodochrosite and barite possible precipitation, as the fluid medium is still oversaturated  
830 regarding these minerals (SI > 0). The increase of dSO<sub>4</sub> (+20%) could be attributed to anhydrite  
831 dissolution (SI < 0), and no more consumption by the *Archaeoglobus* genus. However,  
832 assuming that <sup>87</sup>Sr/<sup>86</sup>Sr ratio of anhydrite is similar to that of the end-member (see section  
833 4.2.1), its dissolution should deliver less radiogenic <sup>87</sup>Sr/<sup>86</sup>Sr ratio to the fluid medium which  
834 is not consistent with the drastic increase of <sup>87</sup>Sr/<sup>86</sup>Sr ratio from 0.707337 to 0.707794 (Fig.  
835 4D).

836  
837 The microbial influence needs to be address. The relative abundance of Deinococci increases,  
838 reaching a level of abundance similar to that of *Sulfurimonas*, and is correlated with a decrease  
839 in dSr concentrations and an increase in <sup>87</sup>Sr/<sup>86</sup>Sr ratios. We suggest that Deinococci trap dSr  
840 through either biosorption or bioaccumulation, and can potentially fractionate the Sr isotope  
841 distribution via its metabolic pathway, leading to progressive radiogenic <sup>87</sup>Sr in the fluid  
842 medium (Fig. 6b). We observe a similar behavior between Sr and Li elemental and isotopic  
843 composition (Fig. 4d and 4e). The δ<sup>7</sup>Li values show a significant and progressive increase over  
844 time, i.e. from +4.6 to +10.3 ‰ (apart at 432 h). This is concomitant with dLi decrease and  
845 Deinococci class taking over the *Sulfurimonas* genus (Fig. 5b). dLi plays a role in many  
846 physiological and biochemical functions of many living organisms (Jakobsson et al., 2017).  
847 Also, dLi could be exchanged through inward flux of H<sup>+</sup> in a regulation of intracellular toxic  
848 metal process (Swartz et al., 2005). Moreover, Poet et al (2023) showed that Li incorporation  
849 through membrane ion channels and Na<sup>+</sup>-Li<sup>+</sup>/H<sup>+</sup> exchangers fractionate Li isotopes  
850 transporting <sup>6</sup>Li faster than <sup>7</sup>Li. Such fractionation process should lead to a heavier δ<sup>7</sup>Li  
851 signature in the fluid which is observed here. Therefore, we suggest that Deinococci trap dLi  
852 leading to a decrease of dLi concentrations and a heavier δ<sup>7</sup>Li signature in the fluid medium.  
853

## 854 5 Conclusion

855 The chemical and isotopic composition of the fluid medium in the gas-lift bioreactor reflects  
856 mineral-fluid-microorganism interactions (Fig. 6). Since the first interaction between buoyant  
857 hydrothermal fluid and the sulfate-based chimney (inoculum, 93% anhydrite), the  
858 microorganism diversity present in both collected material is depleted in favor of that of the  
859 inoculum. Throughout the experiment, Archaeoglobi, Thermoprotei, Thermococci are the main  
860 archaea present in the bioreactor, while *Sulfurimonas* and Deinococci are the main bacteria.  
861 Over the course of the 18-days experiment, the control exerted by microorganisms and minerals  
862 over the chemical composition of the fluid medium evolves. This evolution delineates four  
863 distinct temporal phases: first fluid-inoculum interactions (0 to 24 h), stabilization (24 to 168  
864 h), drastic change (168 to 264 h), and return to stabilization (264 to 432 h). During the first  
865 fluid-inoculum interactions, sulfur-reducing archaea classes (Thermoprotei and Thermococci)  
866 prevail over sulfate-reducing ones (Archaeoglobi). Mineral precipitation (sulfide minerals,  
867 rhodochrosite) and dissolution (anhydrite) seem to control the elemental and isotopic chemical  
868 composition of the fluid medium. During the stabilization (24 to 168 h), bioreactor conditions,  
869 microbial diversity, and most chemical concentrations as well as the Sr isotopic signature of  
870 the fluid remained stable. The slight decrease of dCa, dSO<sub>4</sub>, and dSr concentrations can be  
871 explained by mineral (calcite) precipitation and are coherent with the sulfate-reducing  
872 metabolism of Archaeoglobi. During the drastic change, while Archaeoglobi were less  
873 abundant and the microbial diversity is dominated by sulfur-reducing microorganisms, major  
874 element concentration remains overall constant, trace element concentrations drastically  
875 increase (except dFe), and Sr isotopic ratio drastically decreases. We suggest that Archaeoglobi

876 would have released previously stored trace metals (dSr, dMn, dLi, and dBa) into the fluid  
877 medium leading to less radiogenic  $^{87}\text{Sr}/^{86}\text{Sr}$  ratios. During the return to stabilization interval,  
878 the elementary chemical composition of the fluid is controlled by the carbonate precipitation  
879 and anhydrite dissolution. Increases in the  $^{87}\text{Sr}/^{86}\text{Sr}$  ratio and  $\delta^7\text{Li}$  isotopic signature are  
880 concomitant with the increased abundance of Deinococci, reaching a similar level of abundance  
881 as *Sulfurimonas*. We suggest that Deinococci likely absorb and accumulate dSr and dLi,  
882 leading to the gradual increase in radiogenic  $^{87}\text{Sr}/^{86}\text{Sr}$  ratios and a heavier  $\delta^7\text{Li}$  signature in the  
883 fluid medium.

884 Overall, the evolution of major element concentrations in the fluid medium is controlled by  
885 mineral-fluid interactions, the trace element concentrations are controlled both by minerals and  
886 microorganisms, and the Sr and Li isotopic variations seem to be mainly controlled by  
887 microorganisms (Fig. 6). This underscores the necessity for cautious interpretation when  
888 utilizing Sr isotopes as tracers for paleo hydrothermal records, as they might be affected by  
889 biological isotopic fractionation. Note that Sr isotopic variation effectively highlight mineral-  
890 fluid-microorganisms interactions, whereas the consistent fluctuations in  $\delta^7\text{Li}$  signatures  
891 throughout the experiment complicate its use as a reliable tracer. Further studies focusing on  
892 measuring isotopic fractionation factors in these three compartments are needed to enhance our  
893 understanding of mineral-fluid-microorganism interactions.

894

#### 895 **Author Contribution Statement:**

896

897 AG, DF and FL did the bioreactor experiment and sampling onboard, and the microbial  
898 diversity study onshore. VC, and CD performed the chemical analysis onboard. LA performed  
899 the elemental and isotopic analyses onshore, the PHREEQC geochemical modeling in  
900 collaboration with CD, integrated all data, and performed the visualization/data presentation  
901 work with inputs from the other authors. LA, VC, and CD conducted the interpretation work  
902 and drafted the manuscript with LA leading the writing and with significant contributions from  
903 AG and DF.

#### 904 **Funding**

905 The Institut Carnot ISIFoR through the ADERA provided funding for LA, and VC. The  
906 CNRS/INSU TELLUS 2021 call provided funding for the AMINO project. The EU project  
907 Emso Eric (<http://www.emso-eu.org/>) provided funding for the maintenance of the EMSO-  
908 Azores observatory.

909

#### 910 **Data Availability Statement**

911 The original data presented in the study are included in the main article and in the  
912 Supplementary Material.



## 913 Acknowledgments

914 We thank the *R.V. Pourquoi Pas?* and Genavir crew for their tremendous work during the  
915 MoMARSat'19. We are grateful to the chemistry facility of the Géoscience Environment  
916 Toulouse laboratory (GET), the clean room facility of the Laboratoire d'Etudes en  
917 Géophysique et Océanographie Spatiales (LEGOS), and the mass spectrometry facility of the  
918 PANGEE platform at the Observatoire Midi-Pyrénées (OMP). We thank Céline Rommevaux  
919 for her assistance on board and her feedback on the first draft of this paper.  
920

## 921 References

- 922 Akerman, N., Butterfield, D., & Huber, J. (2013). Phylogenetic diversity and functional gene  
923 patterns of sulfur-oxidizing seafloor Epsilonproteobacteria in diffuse hydrothermal  
924 vent fluids. *Frontiers in Microbiology*, 4.  
925 <https://www.frontiersin.org/articles/10.3389/fmicb.2013.00185>
- 926 Alain, K., Zbinden, M., Le Bris, N., Lesongeur, F., Quérellou, J., Gaill, F., &  
927 Cambon-Bonavita, M. (2004). Early steps in microbial colonization processes at  
928 deep-sea hydrothermal vents. *Environmental Microbiology*, 6(3), 227–241.  
929 <https://doi.org/10.1111/j.1462-2920.2003.00557.x>
- 930 Andrews, M. G., Jacobson, A. D., Lehn, G. O., Horton, T. W., & Craw, D. (2016). Radiogenic  
931 and stable Sr isotope ratios ( $^{87}\text{Sr}/^{86}\text{Sr}$ ,  $\delta^{88/86}\text{Sr}$ ) as tracers of riverine cation  
932 sources and biogeochemical cycling in the Milford Sound region of Fiordland, New  
933 Zealand. *Geochimica et Cosmochimica Acta*, 173, 284–303.  
934 <https://doi.org/10.1016/j.gca.2015.10.005>
- 935 Araoka, D., Nishio, Y., Gamo, T., Yamaoka, K., & Kawahata, H. (2016). Lithium isotopic  
936 systematics of submarine vent fluids from arc and back-arc hydrothermal systems in  
937 the western Pacific. *Geochemistry, Geophysics, Geosystems*, 17(10), 3835–3853.  
938 <https://doi.org/10.1002/2016GC006355>
- 939 Artigue, L., Chavagnac, V., Destrigneville, C., Ferron, B., & Cathalot, C. (2022). Tracking the  
940 Lithium and Strontium Isotope Signature of Hydrothermal Plume in the Water Column:  
941 A Case Study at the EMSO-Azores Deep-Sea Observatory. *Frontiers in Environmental*  
942 *Chemistry*, 3, 784385. <https://doi.org/10.3389/fenvc.2022.784385>
- 943 Astorch-Cardona, A., Guerre, M., Dolla, A., Chavagnac, V., & Rommevaux, C. (2023). Spatial  
944 comparison and temporal evolution of two marine iron-rich microbial mats from the  
945 Lucky Strike Hydrothermal Field, related to environmental variations. *Frontiers in*  
946 *Marine Science*, 10, 1038192. <https://doi.org/10.3389/fmars.2023.1038192>
- 947 Baker, B. J., Lesniewski, R. A., & Dick, G. J. (2012). Genome-enabled transcriptomics reveals  
948 archaeal populations that drive nitrification in a deep-sea hydrothermal plume. *The*  
949 *ISME Journal*, 6(12), 2269–2279. <https://doi.org/10.1038/ismej.2012.64>
- 950 Barker, A. K., Coogan, L. A., Gillis, K. M., & Weis, D. (2008). Strontium isotope constraints  
951 on fluid flow in the sheeted dike complex of fast spreading crust: Pervasive fluid flow  
952 at Pito Deep. *Geochemistry, Geophysics, Geosystems*, 9(6), n/a-n/a.  
953 <https://doi.org/10.1029/2007GC001901>
- 954 Barton, L. L., Fardeau, M.-L., & Fauque, G. D. (2014). Hydrogen Sulfide: A Toxic Gas  
955 Produced by Dissimilatory Sulfate and Sulfur Reduction and Consumed by Microbial  
956 Oxidation. In P. M. H. Kroneck & M. E. S. Torres (Eds.), *The Metal-Driven*  
957 *Biogeochemistry of Gaseous Compounds in the Environment* (Vol. 14, pp. 237–277).  
958 Springer Netherlands. [https://doi.org/10.1007/978-94-017-9269-1\\_10](https://doi.org/10.1007/978-94-017-9269-1_10)
- 959 Bertoldo, C., & Antranikian, G. (2006). The Order Thermococcales. In M. Dworkin, S. Falkow,  
960 E. Rosenberg, K.-H. Schleifer, & E. Stackebrandt (Eds.), *The Prokaryotes: Volume 3:*

- 961 *Archaea. Bacteria: Firmicutes, Actinomycetes* (pp. 69–81). Springer.  
 962 [https://doi.org/10.1007/0-387-30743-5\\_5](https://doi.org/10.1007/0-387-30743-5_5)
- 963 Besson, P., Degboe, J., Berge, B., Chavagnac, V., Fabre, S., & Berger, G. (2014). Calcium, Na,  
 964 K and Mg Concentrations in Seawater by Inductively Coupled Plasma-Atomic  
 965 Emission Spectrometry: Applications to IAPSO Seawater Reference Material,  
 966 Hydrothermal Fluids and Synthetic Seawater Solutions. *Geostandards and*  
 967 *Geoanalytical Research*, 38(3), 355–362. [https://doi.org/10.1111/j.1751-](https://doi.org/10.1111/j.1751-908X.2013.00269.x)  
 968 [908X.2013.00269.x](https://doi.org/10.1111/j.1751-908X.2013.00269.x)
- 969 Bischoff, J. L., & Seyfried, W. E. (1978). Hydrothermal chemistry of seawater from 25 degrees  
 970 to 350 degrees C. *American Journal of Science*, 278(6), 838–860.  
 971 <https://doi.org/10.2475/ajs.278.6.838>
- 972 Boeuf, D., Eppley, J. M., Mende, D. R., Malmstrom, R. R., Woyke, T., & DeLong, E. F. (2021).  
 973 Metapangenomics reveals depth-dependent shifts in metabolic potential for the  
 974 ubiquitous marine bacterial SAR324 lineage. *Microbiome*, 9(1), 172.  
 975 <https://doi.org/10.1186/s40168-021-01119-5>
- 976 Bolyen, E., Rideout, J. R., Dillon, M. R., Bokulich, N. A., Abnet, C. C., Al-Ghalith, G. A.,  
 977 Alexander, H., Alm, E. J., Arumugam, M., Asnicar, F., Bai, Y., Bisanz, J. E., Bittinger,  
 978 K., Brejnrod, A., Brislawn, C. J., Brown, C. T., Callahan, B. J., Caraballo-Rodríguez,  
 979 A. M., Chase, J., ... Caporaso, J. G. (2019). Author Correction: Reproducible,  
 980 interactive, scalable and extensible microbiome data science using QIIME 2. *Nature*  
 981 *Biotechnology*, 37(9), 1091–1091. <https://doi.org/10.1038/s41587-019-0252-6>
- 982 Breier, J. A., White, S. N., & German, C. R. (2010). Mineral–microbe interactions in deep-sea  
 983 hydrothermal systems: A challenge for Raman spectroscopy. *Philosophical*  
 984 *Transactions of the Royal Society A: Mathematical, Physical and Engineering*  
 985 *Sciences*, 368(1922), 3067–3086. <https://doi.org/10.1098/rsta.2010.0024>
- 986 Burger, A., & Lichtscheidl, I. (2019). Strontium in the environment: Review about reactions  
 987 of plants towards stable and radioactive strontium isotopes. *Science of The Total*  
 988 *Environment*, 653, 1458–1512. <https://doi.org/10.1016/j.scitotenv.2018.10.312>
- 989 Burggraf, S., Jannasch, H. W., Nicolaus, B., & Stetter, K. O. (1990). *Archaeoglobus profundus*  
 990 sp. Nov., Represents a New Species within the Sulfate-reducing Archaeobacteria.  
 991 *Systematic and Applied Microbiology*, 13(1), 24–28. [https://doi.org/10.1016/S0723-](https://doi.org/10.1016/S0723-2020(11)80176-1)  
 992 [2020\(11\)80176-1](https://doi.org/10.1016/S0723-2020(11)80176-1)
- 993 Callac, N., Rouxel, O., Lesongeur, F., Liorzou, C., Bollinger, C., Pignet, P., Chéron, S.,  
 994 Fouquet, Y., Rommevaux-Jestin, C., & Godfroy, A. (2015). Biogeochemical insights  
 995 into microbe–mineral–fluid interactions in hydrothermal chimneys using enrichment  
 996 culture. *Extremophiles*, 19(3), 597–617. <https://doi.org/10.1007/s00792-015-0742-5>
- 997 Callahan, B. J., McMurdie, P. J., Rosen, M. J., Han, A. W., Johnson, A. J. A., & Holmes, S. P.  
 998 (2016). DADA2: High resolution sample inference from Illumina amplicon data.  
 999 *Nature Methods*, 13(7), 581–583. <https://doi.org/10.1038/nmeth.3869>
- 1000 Cerqueira, T., Pinho, D., Froufe, H., Santos, R. S., Bettencourt, R., & Egas, C. (2017). Sediment  
 1001 Microbial Diversity of Three Deep-Sea Hydrothermal Vents Southwest of the Azores.  
 1002 *Microbial Ecology*, 74(2), 332–349. <https://doi.org/10.1007/s00248-017-0943-9>
- 1003 Chan, L.-H., & Hein, J. R. (2007). Lithium contents and isotopic compositions of  
 1004 ferromanganese deposits from the global ocean. *Deep Sea Research Part II: Topical*  
 1005 *Studies in Oceanography*, 54(11), 1147–1162.  
 1006 <https://doi.org/10.1016/j.dsr2.2007.04.003>
- 1007 Chandrangsu, P., Rensing, C., & Helmann, J. D. (2017). Metal homeostasis and resistance in  
 1008 bacteria. *Nature Reviews Microbiology*, 15(6), 338–350.  
 1009 <https://doi.org/10.1038/nrmicro.2017.15>

- 1010 Charlou, J. L., Donval, J. P., Douville, E., Jean-Baptiste, P., Radford-Knoery, J., Fouquet, Y.,  
1011 Dapoigny, A., & Stievenard, M. (2000). Compared geochemical signatures and the  
1012 evolution of Menez Gwen (37°50'N) and Lucky Strike (37°17'N) hydrothermal fluids,  
1013 south of the Azores Triple Junction on the Mid-Atlantic Ridge. *Chemical Geology*,  
1014 *171*(1), 49–75. [https://doi.org/10.1016/S0009-2541\(00\)00244-8](https://doi.org/10.1016/S0009-2541(00)00244-8)
- 1015 Chavagnac, V., Leleu, T., Fontaine, F., Cannat, M., Ceuleneer, G., & Castillo, A. (2018).  
1016 Spatial Variations in Vent Chemistry at the Lucky Strike Hydrothermal Field,  
1017 Mid-Atlantic Ridge (37°N): Updates for Subseafloor Flow Geometry From the Newly  
1018 Discovered Capelinhos Vent. *Geochemistry, Geophysics, Geosystems*, *19*(11), 4444–  
1019 4458. <https://doi.org/10.1029/2018GC007765>
- 1020 Chavagnac, V., Saleban Ali, H., Jeandel, C., Leleu, T., Destrigneville, C., Castillo, A., Cotte,  
1021 L., Waeles, M., Cathalot, C., Laes-Huon, A., Pelleter, E., Nonnotte, P., Sarradin, P.-M.,  
1022 & Cannat, M. (2018). Sulfate minerals control dissolved rare earth element flux and Nd  
1023 isotope signature of buoyant hydrothermal plume (EMSO-Azores, 37°N Mid-Atlantic  
1024 Ridge). *Chemical Geology*, *499*, 111–125.  
1025 <https://doi.org/10.1016/j.chemgeo.2018.09.021>
- 1026 Chowdhury, M. J., & Blust, R. (2011). 7—Strontium. In C. M. Wood, A. P. Farrell, & C. J.  
1027 Brauner (Eds.), *Fish Physiology* (Vol. 31, pp. 351–390). Academic Press.  
1028 [https://doi.org/10.1016/S1546-5098\(11\)31029-1](https://doi.org/10.1016/S1546-5098(11)31029-1)
- 1029 Crépeau, V., Cambon Bonavita, M.-A., Lesongeur, F., Randrianalivelo, H., Sarradin, P.-M.,  
1030 Sarrazin, J., & Godfroy, A. (2011). Diversity and function in microbial mats from the  
1031 Lucky Strike hydrothermal vent field: Diversity and function in Lucky Strike mats.  
1032 *FEMS Microbiology Ecology*, *76*(3), 524–540. [https://doi.org/10.1111/j.1574-](https://doi.org/10.1111/j.1574-6941.2011.01070.x)  
1033 [6941.2011.01070.x](https://doi.org/10.1111/j.1574-6941.2011.01070.x)
- 1034 Davis, A. C., Bickle, M. J., & Teagle, D. A. H. (2003). Imbalance in the oceanic strontium  
1035 budget. *Earth and Planetary Science Letters*, *211*(1), 173–187.  
1036 [https://doi.org/10.1016/S0012-821X\(03\)00191-2](https://doi.org/10.1016/S0012-821X(03)00191-2)
- 1037 Dick, G. J., Anantharaman, K., Baker, B. J., Li, M., Reed, D. C., & Sheik, C. S. (2013). The  
1038 microbiology of deep-sea hydrothermal vent plumes: Ecological and biogeographic  
1039 linkages to seafloor and water column habitats. *Frontiers in Microbiology*, *4*.  
1040 <https://doi.org/10.3389/fmicb.2013.00124>
- 1041 Dick, G. J., & Tebo, B. M. (2010). Microbial diversity and biogeochemistry of the Guaymas  
1042 Basin deep-sea hydrothermal plume. *Environmental Microbiology*, *12*(5), 1334–1347.  
1043 <https://doi.org/10.1111/j.1462-2920.2010.02177.x>
- 1044 Edwards, K. J., Bach, W., & McCollom, T. M. (2005). Geomicrobiology in oceanography:  
1045 Microbe–mineral interactions at and below the seafloor. *Trends in Microbiology*, *13*(9),  
1046 449–456. <https://doi.org/10.1016/j.tim.2005.07.005>
- 1047 El Meknassi, S., Dera, G., De Rafélis, M., Brahmi, C., Lartaud, F., Hodel, F., Jeandel, C.,  
1048 Menjot, L., Mounic, S., Henry, M., Besson, P., & Chavagnac, V. (2020). Seawater  
1049 <sup>87</sup>Sr/<sup>86</sup>Sr ratios along continental margins: Patterns and processes in open and  
1050 restricted shelf domains. *Chemical Geology*, *558*, 119874.  
1051 <https://doi.org/10.1016/j.chemgeo.2020.119874>
- 1052 Elderfield, H., & Schultz, A. (1996). Mid-Ocean Ridge Hydrothermal Fluxes and the Chemical  
1053 Composition of the Ocean. *Annual Review of Earth and Planetary Science*, *24*, 191–  
1054 224. <https://doi.org/10.1146/annurev.earth.24.1.191>
- 1055 Escartin, J., Barreyre, T., Cannat, M., Garcia, R., Gracias, N., Deschamps, A., Salocchi, A.,  
1056 Sarradin, P.-M., & Ballu, V. (2015). Hydrothermal activity along the slow-spreading  
1057 Lucky Strike ridge segment (Mid-Atlantic Ridge): Distribution, heatflux, and  
1058 geological controls. *Earth and Planetary Science Letters*, *431*, 173–185.  
1059 <https://doi.org/10.1016/j.epsl.2015.09.025>

- 1060 *European Commission, Study on the EU's list of Critical Raw Materials – Final Report.* (2020).
- 1061 Flores, G. E., Campbell, J. H., Kirshtein, J. D., Meneghin, J., Podar, M., Steinberg, J. I.,
- 1062 Seewald, J. S., Tivey, M. K., Voytek, M. A., Yang, Z. K., & Reysenbach, A.-L. (2011).
- 1063 Microbial community structure of hydrothermal deposits from geochemically different
- 1064 vent fields along the Mid-Atlantic Ridge: Microbial communities of hydrothermal vent
- 1065 deposits. *Environmental Microbiology*, 13(8), 2158–2171.
- 1066 <https://doi.org/10.1111/j.1462-2920.2011.02463.x>
- 1067 Fouquet, Y., Ondréas, H., Charlou, J.-L., Donval, J.-P., Radford-Knoery, J., Costa, I.,
- 1068 Lourenço, N., M. K., T., & Tivey, M. K. (1995). Atlantic lava lakes and hot vents.
- 1069 *Nature*, 377(6546), 201–201. <https://doi.org/10.1038/377201a0>
- 1070 François, D. (2021). *Spatial and temporal dynamics of microbial communities in active*
- 1071 *hydrothermal vents.* Université de Bretagne Occidentale.
- 1072 François, D. X., Godfroy, A., Mathien, C., Aubé, J., Cathalot, C., Lesongeur, F., L'Haridon,
- 1073 S., Philippon, X., & Roussel, E. G. (2021). *Persephonella atlantica* sp. nov.: How to
- 1074 adapt to physico-chemical gradients in high temperature hydrothermal habitats.
- 1075 *Systematic and Applied Microbiology*, 44(1), 126176.
- 1076 <https://doi.org/10.1016/j.syapm.2020.126176>
- 1077 Füger, A., Konrad, F., Leis, A., Dietzel, M., & Mavromatis, V. (2019). Effect of growth rate
- 1078 and pH on lithium incorporation in calcite. *Geochimica et Cosmochimica Acta*, 248,
- 1079 14–24. <https://doi.org/10.1016/j.gca.2018.12.040>
- 1080 Füger, A., Kuessner, M., Rollion-Bard, C., Leis, A., Magna, T., Dietzel, M., & Mavromatis,
- 1081 V. (2022). Effect of growth rate and pH on Li isotope fractionation during its
- 1082 incorporation in calcite. *Geochimica et Cosmochimica Acta*, 323, 276–290.
- 1083 <https://doi.org/10.1016/j.gca.2022.02.014>
- 1084 Garrity, G. M., Bell, J. A., & Lilburn, T. (2005). Class I. Alphaproteobacteria class. Nov. In D.
- 1085 J. Brenner, N. R. Krieg, & J. T. Staley (Eds.), *Bergey's Manual® of Systematic*
- 1086 *Bacteriology: Volume Two The Proteobacteria Part C The Alpha-, Beta-, Delta-, and*
- 1087 *Epsilonproteobacteria* (Vol. 1–garrity, pp. 1–574). Springer US.
- 1088 [https://doi.org/10.1007/978-0-387-29298-4\\_1](https://doi.org/10.1007/978-0-387-29298-4_1)
- 1089 German, C. R., Casciotti, K. A., Dutay, J.-C., Heimbürger, L. E., Jenkins, W. J., Measures, C.
- 1090 I., Mills, R. A., Obata, H., Schlitzer, R., Tagliabue, A., Turner, D. R., & Whitby, H.
- 1091 (2016). Hydrothermal impacts on trace element and isotope ocean biogeochemistry.
- 1092 *Philosophical Transactions of the Royal Society A: Mathematical, Physical and*
- 1093 *Engineering Sciences*, 374(2081), 20160035. <https://doi.org/10.1098/rsta.2016.0035>
- 1094 Godfroy, A., Postec, A., & Raven, N. (2006). 4 Growth of Hyperthermophilic Microorganisms
- 1095 for Physiological and Nutritional Studies. In *Methods in Microbiology* (Vol. 35, pp. 93–
- 1096 108). Elsevier. [https://doi.org/10.1016/S0580-9517\(08\)70007-2](https://doi.org/10.1016/S0580-9517(08)70007-2)
- 1097 Godfroy, A., Raven, N. D. H., & Sharp, R. J. (2000). Physiology and continuous culture of the
- 1098 hyperthermophilic deep-sea vent archaeon *Pyrococcus abyssi* ST549. *FEMS*
- 1099 *Microbiology Letters*, 186(1), 127–132. [https://doi.org/10.1111/j.1574-](https://doi.org/10.1111/j.1574-6968.2000.tb09093.x)
- 1100 [6968.2000.tb09093.x](https://doi.org/10.1111/j.1574-6968.2000.tb09093.x)
- 1101 Gómez-Pereira, P. R., Fuchs, B. M., Alonso, C., Oliver, M. J., van Beusekom, J. E. E., &
- 1102 Amann, R. (2010). Distinct flavobacterial communities in contrasting water masses of
- 1103 the North Atlantic Ocean. *The ISME Journal*, 4(4), 472–487.
- 1104 <https://doi.org/10.1038/ismej.2009.142>
- 1105 Hafenbradl, D., Keller, M., Dirmeier, R., Rachel, R., Roßnagel, P., Burggraf, S., Huber, H., &
- 1106 Stetter, K. O. (1996). *Ferroglobus placidus* gen. Nov., sp. Nov., a novel
- 1107 hyperthermophilic archaeum that oxidizes Fe 2+ at neutral pH under anoxic conditions.
- 1108 *Archives of Microbiology*, 166(5), 308–314. <https://doi.org/10.1007/s002030050388>

- 1109 Haro-Moreno, J. M., Rodriguez-Valera, F., López-García, P., Moreira, D., & Martin-Cuadrado,  
 1110 A.-B. (2017). New insights into marine group III Euryarchaeota, from dark to light. *The*  
 1111 *ISME Journal*, 11(5), 1102–1117. <https://doi.org/10.1038/ismej.2016.188>
- 1112 Hartzell, P., & Reed, D. W. (2006). The Genus *Archaeoglobus*. In M. Dworkin, S. Falkow, E.  
 1113 Rosenberg, K.-H. Schleifer, & E. Stackebrandt (Eds.), *The Prokaryotes: Volume 3:*  
 1114 *Archaea. Bacteria: Firmicutes, Actinomycetes* (pp. 82–100). Springer.  
 1115 [https://doi.org/10.1007/0-387-30743-5\\_6](https://doi.org/10.1007/0-387-30743-5_6)
- 1116 Herlemann, D. P., Labrenz, M., Jürgens, K., Bertilsson, S., Waniek, J. J., & Andersson, A. F.  
 1117 (2011). Transitions in bacterial communities along the 2000 km salinity gradient of the  
 1118 Baltic Sea. *The ISME Journal*, 5(10), 1571–1579.  
 1119 <https://doi.org/10.1038/ismej.2011.41>
- 1120 Hindshaw, R. S., Tosca, R., Goût, T. L., Farnan, I., Tosca, N. J., & Tipper, E. T. (2019).  
 1121 Experimental constraints on Li isotope fractionation during clay formation. *Geochimica*  
 1122 *et Cosmochimica Acta*, 250, 219–237. <https://doi.org/10.1016/j.gca.2019.02.015>
- 1123 Holden, J., Breier, J., Rogers, K., Schulte, M., & Toner, B. (2012). Biogeochemical Processes  
 1124 at Hydrothermal Vents: Microbes and Minerals, Bioenergetics, and Carbon Fluxes.  
 1125 *Oceanography*, 25(1), 196–208. <https://doi.org/10.5670/oceanog.2012.18>
- 1126 Hong, H.-J., Park, I.-S., Ryu, T., Jeong, H. S., & Ryu, J. (2018). Demonstration of Seawater  
 1127 Strontium (Sr(II)) Extraction and Enrichment by a Biosorption Technique through  
 1128 Continuous Column Operation. *Industrial & Engineering Chemistry Research*, 57(38),  
 1129 12909–12915. <https://doi.org/10.1021/acs.iecr.8b02895>
- 1130 Hu, Q., Wang, S., Lai, Q., Shao, Z., & Jiang, L. (2021). *Sulfurimonas indica* sp. Nov., a  
 1131 hydrogen- and sulfur-oxidizing chemolithoautotroph isolated from a hydrothermal  
 1132 sulfide chimney in the Northwest Indian Ocean. *International Journal of Systematic*  
 1133 *and Evolutionary Microbiology*, 71(1). <https://doi.org/10.1099/ijsem.0.004575>
- 1134 Huber, H., Jannasch, H., Rachel, R., Fuchs, T., & Stetter, K. O. (1997). *Archaeoglobus*  
 1135 *veneficus* sp. Nov., a Novel Facultative Chemolithoautotrophic Hyperthermophilic  
 1136 Sulfite Reducer, Isolated from Abyssal Black Smokers. *Systematic and Applied*  
 1137 *Microbiology*, 20(3), 374–380. [https://doi.org/10.1016/S0723-2020\(97\)80005-7](https://doi.org/10.1016/S0723-2020(97)80005-7)
- 1138 Huber, H., & Stetter, K. O. (2006). Desulfurococcales. In M. Dworkin, S. Falkow, E.  
 1139 Rosenberg, K.-H. Schleifer, & E. Stackebrandt (Eds.), *The Prokaryotes: Volume 3:*  
 1140 *Archaea. Bacteria: Firmicutes, Actinomycetes* (pp. 52–68). Springer.  
 1141 [https://doi.org/10.1007/0-387-30743-5\\_4](https://doi.org/10.1007/0-387-30743-5_4)
- 1142 Huber, H., & Stetter, K. O. (2015a). *Archaeoglobus*. In *Bergey's Manual of Systematics of*  
 1143 *Archaea and Bacteria* (pp. 1–5). John Wiley & Sons, Ltd.  
 1144 <https://doi.org/10.1002/9781118960608.gbm00479>
- 1145 Huber, H., & Stetter, K. O. (2015b). Desulfurococcales ord. Nov. In *Bergey's Manual of*  
 1146 *Systematics of Archaea and Bacteria* (pp. 1–2). John Wiley & Sons, Ltd.  
 1147 <https://doi.org/10.1002/9781118960608.obm00040>
- 1148 Huber, J. A., Butterfield, D. A., & Baross, J. A. (2006). Diversity and distribution of  
 1149 subsurface Thermococcales populations in diffuse hydrothermal vents at an active  
 1150 deep-sea volcano in the northeast Pacific Ocean. *Journal of Geophysical Research:*  
 1151 *Biogeosciences*, 111(G4). <https://doi.org/10.1029/2005JG000097>
- 1152 Humphris, S. E., & Bach, W. (2005). Strontium concentrations and isotopic compositions of  
 1153 anhydrites from the TAG active mound [Data set]. In *Supplement to: Humphris, SE;*  
 1154 *Bach, W (2005): On the Sr isotope and REE compositions of anhydrites from the TAG*  
 1155 *seafloor hydrothermal system. Geochimica et Cosmochimica Acta*, 69(6), 1511–1525,  
 1156 <https://doi.org/10.1016/j.gca.2004.10.004>. PANGAEA.  
 1157 <https://doi.org/10.1594/PANGAEA.710795>

- 1158 Inagaki, F. (2003). *Sulfurimonas autotrophica* gen. Nov., sp. Nov., a novel sulfur-oxidizing -  
1159 proteobacterium isolated from hydrothermal sediments in the Mid-Okinawa Trough.  
1160 *INTERNATIONAL JOURNAL OF SYSTEMATIC AND EVOLUTIONARY*  
1161 *MICROBIOLOGY*, 53(6), 1801–1805. <https://doi.org/10.1099/ijms.0.02682-0>
- 1162 Jakobsson, E., Argüello-Miranda, O., Chiu, S.-W., Fazal, Z., Kruczek, J., Nunez-Corrales, S.,  
1163 Pandit, S., & Pritchett, L. (2017). Towards a Unified Understanding of Lithium Action  
1164 in Basic Biology and its Significance for Applied Biology. *The Journal of Membrane*  
1165 *Biology*, 250(6), 587–604. <https://doi.org/10.1007/s00232-017-9998-2>
- 1166 James, R. H., & Palmer, M. R. (2000). The lithium isotope composition of international rock  
1167 standards. *Chemical Geology*, 166(3–4), 319–326. <https://doi.org/10.1016/S0009->  
1168 [2541\(99\)00217-X](https://doi.org/10.1016/S0009-2541(99)00217-X)
- 1169 Jeanthon, C., L'Haridon, S., Pradel, N., & Prieur, D. (1999). Rapid identification of  
1170 hyperthermophilic methanococci isolated from deep-sea hydrothermal vents.  
1171 *International Journal of Systematic and Evolutionary Microbiology*, 49(2), 591–594.  
1172 <https://doi.org/10.1099/00207713-49-2-591>
- 1173 Ji, T.-T., Jiang, X.-W., Gou, L.-F., Jin, Z., Zhang, H., Wan, L., Han, G., Guo, H., & Wang,  
1174 X.-S. (2022). Behaviors of lithium and its isotopes in groundwater with different  
1175 concentrations of dissolved CO<sub>2</sub>. *Geochimica et Cosmochimica Acta*, 326, 313–327.  
1176 <https://doi.org/10.1016/j.gca.2022.03.038>
- 1177 Johnson, J. W., Oelkers, E. H., & Helgeson, H. C. (1992). SUPCRT92: A software package for  
1178 calculating the standard molal thermodynamic properties of minerals, gases, aqueous  
1179 species, and reactions from 1 to 5000 bar and 0 to 1000°C. *Computers & Geosciences*,  
1180 18(7), 899–947. [https://doi.org/10.1016/0098-3004\(92\)90029-Q](https://doi.org/10.1016/0098-3004(92)90029-Q)
- 1181 Jones, W. J., Leigh, J. A., Mayer, F., Woese, C. R., & Wolfe, R. S. (1983). *Methanococcus*  
1182 *jannaschii* sp. Nov., an extremely thermophilic methanogen from a submarine  
1183 hydrothermal vent. *Archives of Microbiology*, 136(4), 254–261.  
1184 <https://doi.org/10.1007/BF00425213>
- 1185 Jones, W. J., Stugard, C. E., & Jannasch, H. W. (1989). Comparison of thermophilic  
1186 methanogens from submarine hydrothermal vents. *Archives of Microbiology*, 151(4),  
1187 314–318. <https://doi.org/10.1007/BF00406557>
- 1188 Kashefi, K., Tor, J. M., Holmes, D. E., Gaw Van Praagh, C. V., Reysenbach, A.-L., & Lovley,  
1189 D. R. (2002). *Geoglobus ahangari* gen. Nov., sp. Nov., a novel hyperthermophilic  
1190 archaeon capable of oxidizing organic acids and growing autotrophically on hydrogen  
1191 with Fe(III) serving as the sole electron acceptor. *INTERNATIONAL JOURNAL OF*  
1192 *SYSTEMATIC AND EVOLUTIONARY MICROBIOLOGY*, 52(3), 719–728.  
1193 <https://doi.org/10.1099/ijms.0.01953-0>
- 1194 Könneke, M., Bernhard, A. E., de la Torre, J. R., Walker, C. B., Waterbury, J. B., & Stahl, D.  
1195 A. (2005). Isolation of an autotrophic ammonia-oxidizing marine archaeon. *Nature*,  
1196 437(7058), 543–546. <https://doi.org/10.1038/nature03911>
- 1197 Langmuir, C., Humphris, S., Fornari, D., Van Dover, C., Von Damm, K., Tivey, M. K.,  
1198 Colodner, D., Charlou, J.-L., Desonie, D., Wilson, C., Fouquet, Y., Klinkhammer, G.,  
1199 & Bougault, H. (1997). Hydrothermal vents near a mantle hot spot: The Lucky Strike  
1200 vent field at 37°N on the Mid-Atlantic Ridge. *Earth and Planetary Science Letters*,  
1201 148(1–2), 69–91. [https://doi.org/10.1016/S0012-821X\(97\)00027-7](https://doi.org/10.1016/S0012-821X(97)00027-7)
- 1202 Le Guellec, S., Leroy, E., Courtine, D., Godfroy, A., & Roussel, E. G. (2021). H<sub>2</sub>-dependent  
1203 formate production by hyperthermophilic Thermococcales: An alternative to sulfur  
1204 reduction for reducing-equivalents disposal. *The ISME Journal*, 1–14.  
1205 <https://doi.org/10.1038/s41396-021-01020-x>

- 1206 Leleu, T. (2017). *Variabilité spatio-temporelle de la composition des fluides hydrothermaux*  
1207 *(observatoire fond de mer EMSO-Açores, Lucky Strike): Traçage de la circulation*  
1208 *hydrothermale et quantification des flux chimiques associés*. UT3 Paul Sabatier.
- 1209 Lepage, E., Marguet, E., Geslin, C., Matte-Tailliez, O., Zillig, W., Forterre, P., & Tailliez, P.  
1210 (2004). Molecular Diversity of New Thermococcales Isolates from a Single Area of  
1211 Hydrothermal Deep-Sea Vents as Revealed by Randomly Amplified Polymorphic  
1212 DNA Fingerprinting and 16S rRNA Gene Sequence Analysis. *Applied and*  
1213 *Environmental Microbiology*, 70(3), 1277–1286.  
1214 <https://doi.org/10.1128/AEM.70.3.1277-1286.2004>
- 1215 Li, J., Yang, J., Sun, M., Su, L., Wang, H., Gao, J., & Bai, S. (2020). Distribution and  
1216 Succession of Microbial Communities Along the Dispersal Pathway of Hydrothermal  
1217 Plumes on the Southwest Indian Ridge. *Frontiers in Marine Science*, 7.  
1218 <https://www.frontiersin.org/articles/10.3389/fmars.2020.581381>
- 1219 Li, W., & Liu, X.-M. (2020). Experimental investigation of lithium isotope fractionation during  
1220 kaolinite adsorption: Implications for chemical weathering. *Geochimica et*  
1221 *Cosmochimica Acta*, 284, 156–172. <https://doi.org/10.1016/j.gca.2020.06.025>
- 1222 Lim, J. K., Kim, Y. J., Yang, J.-A., Namirimu, T., Yang, S.-H., Park, M.-J., Kwon, Y. M., Lee,  
1223 H. S., Kang, S. G., Lee, J.-H., & Kwon, K. K. (2020). Thermococcus indicus sp. Nov.,  
1224 a Fe(III)-reducing hyperthermophilic archaeon isolated from the Onnuri Vent Field of  
1225 the Central Indian Ocean ridge. *Journal of Microbiology*, 58(4), 260–267.  
1226 <https://doi.org/10.1007/s12275-020-9424-9>
- 1227 Liu, Y., Beer, L. L., & Whitman, W. B. (2012). Sulfur metabolism in archaea reveals novel  
1228 processes: Sulfur metabolism in archaea. *Environmental Microbiology*, 14(10), 2632–  
1229 2644. <https://doi.org/10.1111/j.1462-2920.2012.02783.x>
- 1230 Marriott, C. S., Henderson, G. M., Belshaw, N. S., & Tudhope, A. W. (2004). Temperature  
1231 dependence of  $\delta^{7}\text{Li}$ ,  $\delta^{44}\text{Ca}$  and Li/Ca during growth of calcium carbonate. *Earth and*  
1232 *Planetary Science Letters*, 222(2), 615–624. <https://doi.org/10.1016/j.epsl.2004.02.031>
- 1233 Marriott, C. S., Henderson, G. M., Crompton, R., Staubwasser, M., & Shaw, S. (2004). Effect  
1234 of mineralogy, salinity, and temperature on Li/Ca and Li isotope composition of  
1235 calcium carbonate. *Chemical Geology*, 212(1), 5–15.  
1236 <https://doi.org/10.1016/j.chemgeo.2004.08.002>
- 1237 Martin, M. (2011). Cutadapt removes adapter sequences from high-throughput sequencing  
1238 reads. *EMBnet Journal*, 17(1), 10–12.
- 1239 McCliment, E. A., Voglesonger, K. M., O'Day, P. A., Dunn, E. E., Holloway, J. R., & Cary,  
1240 S. C. (2006). Colonization of nascent, deep-sea hydrothermal vents by a novel Archaeal  
1241 and Nanoarchaeal assemblage. *Environmental Microbiology*, 8(1), 114–125.  
1242 <https://doi.org/10.1111/j.1462-2920.2005.00874.x>
- 1243 Millero, F. J., Feistel, R., Wright, D. G., & McDougall, T. J. (2008). The composition of  
1244 Standard Seawater and the definition of the Reference-Composition Salinity Scale.  
1245 *Deep Sea Research Part I: Oceanographic Research Papers*, 55(1), 50–72.  
1246 <https://doi.org/10.1016/j.dsr.2007.10.001>
- 1247 Millot, R., Scaillet, B., & Sanjuan, B. (2010). Lithium isotopes in island arc geothermal  
1248 systems: Guadeloupe, Martinique (French West Indies) and experimental approach.  
1249 *Geochimica et Cosmochimica Acta*, 74(6), 1852–1871.  
1250 <https://doi.org/10.1016/j.gca.2009.12.007>
- 1251 Mino, S., Nakagawa, S., Makita, H., Toki, T., Miyazaki, J., Sievert, S. M., Polz, M. F., Inagaki,  
1252 F., Godfroy, A., Kato, S., Watanabe, H., Nunoura, T., Nakamura, K., Imachi, H.,  
1253 Watsuji, T., Kojima, S., Takai, K., & Sawabe, T. (2017). Endemicity of the  
1254 cosmopolitan mesophilic chemolithoautotroph Sulfurimonas at deep-sea hydrothermal  
1255 vents. *The ISME Journal*, 11(4), 909–919. <https://doi.org/10.1038/ismej.2016.178>

- 1256 Miroshnichenko, M. L., L'Haridon, S., Nercessian, O., Antipov, A. N., Kostrikina, N. A.,  
 1257 Tindall, B. J., Schumann, P., Spring, S., Stackebrandt, E., Bonch-Osmolovskaya, E. A.,  
 1258 & Jeanthon, C. (2003). *Vulcanithermus mediatlanticus* gen. Nov., sp. Nov., a novel  
 1259 member of the family Thermaceae from a deep-sea hot vent. *International Journal of*  
 1260 *Systematic and Evolutionary Microbiology*, 53(4), 1143–1148.  
 1261 <https://doi.org/10.1099/ijs.0.02579-0>
- 1262 Molari, M., Hassenrueck, C., Laso-Pérez, R., Wegener, G., Offre, P., Scilipoti, S., & Boetius,  
 1263 A. (2023). A hydrogenotrophic Sulfurimonas is globally abundant in deep-sea oxygen-  
 1264 saturated hydrothermal plumes. *Nature Microbiology*, 8(4), 651–665.  
 1265 <https://doi.org/10.1038/s41564-023-01342-w>
- 1266 Mori, K., Maruyama, A., Urabe, T., Suzuki, K. -i., & Hanada, S. (2008). *Archaeoglobus*  
 1267 *infectus* sp. Nov., a novel thermophilic, chemolithoheterotrophic archaeon isolated  
 1268 from a deep-sea rock collected at Suiyo Seamount, Izu-Bonin Arc, western Pacific  
 1269 Ocean. *INTERNATIONAL JOURNAL OF SYSTEMATIC AND EVOLUTIONARY*  
 1270 *MICROBIOLOGY*, 58(4), 810–816. <https://doi.org/10.1099/ijs.0.65422-0>
- 1271 Morris, R. M., Rappé, M. S., Connon, S. A., Vergin, K. L., Siebold, W. A., Carlson, C. A., &  
 1272 Giovannoni, S. J. (2002). SAR11 clade dominates ocean surface bacterioplankton  
 1273 communities. *Nature*, 420(6917), 806–810. <https://doi.org/10.1038/nature01240>
- 1274 Nakagawa, S., Takai, K., Inagaki, F., Hirayama, H., Nunoura, T., Horikoshi, K., & Sako, Y.  
 1275 (2005). Distribution, phylogenetic diversity and physiological characteristics of  
 1276 epsilon-Proteobacteria in a deep-sea hydrothermal field. *Environmental Microbiology*,  
 1277 7(10), 1619–1632. <https://doi.org/10.1111/j.1462-2920.2005.00856.x>
- 1278 Neymark, L. A., Premo, W. R., Mel'nikov, N. N., & Emsbo, P. (2014). *Precise determination*  
 1279 *of d88Sr in rocks, minerals, and waters by double-spike TIMS: a powerful tool in the*  
 1280 *study of geological, hydrological and biological processes*. 11.
- 1281 Offre, P., Spang, A., & Schleper, C. (2013). Archaea in Biogeochemical Cycles. *Annual Review*  
 1282 *of Microbiology*, 67(1), 437–457. <https://doi.org/10.1146/annurev-micro-092412-155614>
- 1284 Olesen, S. W., Duvallet, C., & Alm, E. J. (2017). dbOTU3: A new implementation of  
 1285 distribution-based OTU calling. *PLOS ONE*, 12(5), e0176335.  
 1286 <https://doi.org/10.1371/journal.pone.0176335>
- 1287 Ondréas, H., Cannat, M., Fouquet, Y., Normand, A., Sarradin, P. M., & Sarrazin, J. (2009).  
 1288 Recent volcanic events and the distribution of hydrothermal venting at the Lucky Strike  
 1289 hydrothermal field, Mid-Atlantic Ridge. *Geochemistry, Geophysics, Geosystems*,  
 1290 10(2). <https://doi.org/10.1029/2008GC002171>
- 1291 Pagé, A., Tivey, M. K., Stakes, D. S., & Reysenbach, A.-L. (2008). Temporal and spatial  
 1292 archaeal colonization of hydrothermal vent deposits. *Environmental Microbiology*,  
 1293 10(4), 874–884. <https://doi.org/10.1111/j.1462-2920.2007.01505.x>
- 1294 Parkhurst, D. L., & Appelo, C. A. J. (2013). Description of input and examples for PHREEQC  
 1295 version 3: A computer program for speciation, batch-reaction, one-dimensional  
 1296 transport, and inverse geochemical calculations. In *Description of input and examples*  
 1297 *for PHREEQC version 3: A computer program for speciation, batch-reaction, one-*  
 1298 *dimensional transport, and inverse geochemical calculations* (USGS Numbered Series  
 1299 No. 6-A43; Techniques and Methods, Vols. 6-A43, p. 519). U.S. Geological Survey.  
 1300 <https://doi.org/10.3133/tm6A43>
- 1301 Pester, N. J., Reeves, E. P., Rough, M. E., Ding, K., Seewald, J. S., & Seyfried, W. E. (2012).  
 1302 Subseafloor phase equilibria in high-temperature hydrothermal fluids of the Lucky  
 1303 Strike Seamount (Mid-Atlantic Ridge, 37°17'N). *Geochimica et Cosmochimica Acta*,  
 1304 90, 303–322. <https://doi.org/10.1016/j.gca.2012.05.018>



- 1305 Pin, C., Gannoun, A., & Dupont, A. (2014). Rapid, simultaneous separation of Sr, Pb, and Nd  
 1306 by extraction chromatography prior to isotope ratios determination by TIMS and MC-  
 1307 ICP-MS. *Journal of Analytical Atomic Spectrometry*, 29.  
 1308 <https://doi.org/10.1039/C4JA00169A>
- 1309 Poet, M., Vigier, N., Bouret, Y., Jarretou, G., Gautier, R., Bendahhou, S., Balter, V., Montanes,  
 1310 M., Thibon, F., & Counillon, L. (2023). Biological fractionation of lithium isotopes by  
 1311 cellular Na<sup>+</sup>/H<sup>+</sup> exchangers unravels fundamental transport mechanisms. *iScience*,  
 1312 26(6). <https://doi.org/10.1016/j.isci.2023.106887>
- 1313 Postec, A., Lesongeur, F., Pignet, P., Ollivier, B., Querellou, J., & Godfroy, A. (2007).  
 1314 Continuous enrichment cultures: Insights into prokaryotic diversity and metabolic  
 1315 interactions in deep-sea vent chimneys. *Extremophiles*, 11(6), 747–757.  
 1316 <https://doi.org/10.1007/s00792-007-0092-z>
- 1317 Postec, A., Pignet, P., Cuffe-Gauchard, V., Schmitt, A., Querellou, J., & Godfroy, A. (2005).  
 1318 Optimisation of growth conditions for continuous culture of the hyperthermophilic  
 1319 archaeon *Thermococcus hydrothermalis* and development of sulphur-free defined and  
 1320 minimal media. *Research in Microbiology*, 156(1), 82–87.  
 1321 <https://doi.org/10.1016/j.resmic.2004.08.001>
- 1322 Postec, A., Urios, L., Lesongeur, F., Ollivier, B., Querellou, J., & Godfroy, A. (2005).  
 1323 Continuous Enrichment Culture and Molecular Monitoring to Investigate the Microbial  
 1324 Diversity of Thermophiles Inhabiting Deep-Sea Hydrothermal Ecosystems. *Current*  
 1325 *Microbiology*, 50(3), 138–144. <https://doi.org/10.1007/s00284-004-4443-z>
- 1326 Qin, W., Heal, K. R., Ramdasi, R., Kobelt, J. N., Martens-Habbena, W., Bertagnolli, A. D.,  
 1327 Amin, S. A., Walker, C. B., Urakawa, H., Könneke, M., Devol, A. H., Moffett, J. W.,  
 1328 Armbrust, E. V., Jensen, G. J., Ingalls, A. E., & Stahl, D. A. (2017). *Nitrosopumilus*  
 1329 *maritimus* gen. Nov., sp. Nov., *Nitrosopumilus cobalaminigenes* sp. Nov.,  
 1330 *Nitrosopumilus oxyclineae* sp. Nov., and *Nitrosopumilus ureiphilus* sp. Nov., four  
 1331 marine ammonia-oxidizing archaea of the phylum Thaumarchaeota. *International*  
 1332 *Journal of Systematic and Evolutionary Microbiology*, 67(12), 5067–5079.  
 1333 <https://doi.org/10.1099/ijsem.0.002416>
- 1334 Qin, W., Martens-Habbena, W., Kobelt, J. N., & Stahl, D. A. (2016). *Candidatus*  
 1335 *Nitrosopumilus*. In W. B. Whitman, F. Rainey, P. Kämpfer, M. Trujillo, J. Chun, P.  
 1336 DeVos, B. Hedlund, & S. Dedysh (Eds.), *Bergey's Manual of Systematics of Archaea*  
 1337 *and Bacteria* (1st ed., pp. 1–9). Wiley.  
 1338 <https://doi.org/10.1002/9781118960608.gbm01290>
- 1339 Quast, C., Pruesse, E., Yilmaz, P., Gerken, J., Schweer, T., Yarza, P., Peplies, J., & Glöckner,  
 1340 F. O. (2012). The SILVA ribosomal RNA gene database project: Improved data  
 1341 processing and web-based tools. *Nucleic Acids Research*, 41(D1), D590–D596.  
 1342 <https://doi.org/10.1093/nar/gks1219>
- 1343 Rappé, M. S., Connon, S. A., Vergin, K. L., & Giovannoni, S. J. (2002). Cultivation of the  
 1344 ubiquitous SAR11 marine bacterioplankton clade. *Nature*, 418(6898), 630–633.  
 1345 <https://doi.org/10.1038/nature00917>
- 1346 Raven, N., Ladwa, N., Cossar, D., & Sharp, R. (1992). Continuous culture of the  
 1347 hyperthermophilic archaeum *Pyrococcus furiosus*. *Applied Microbiology and*  
 1348 *Biotechnology*, 38(2), 263–267. <https://doi.org/10.1007/BF00174480>
- 1349 Reysenbach, A.-L., Huber, R., Stetter, K. O., Ishii, M., Kawasumi, T., Igarashi, Y., Eder, W.,  
 1350 L'Haridon, S., & Jeanthon, C. (2001). Phylum BI. Aquificae phy. Nov. In D. R. Boone,  
 1351 R. W. Castenholz, & G. M. Garrity (Eds.), *Bergey's Manual® of Systematic*  
 1352 *Bacteriology: Volume One: The Archaea and the Deeply Branching and Phototrophic*  
 1353 *Bacteria* (pp. 359–367). Springer. [https://doi.org/10.1007/978-0-387-21609-6\\_18](https://doi.org/10.1007/978-0-387-21609-6_18)

- 1354 Reysenbach, A.-L., Liu, Y., Banta, A. B., Beveridge, T. J., Kirshtein, J. D., Schouten, S., Tivey,  
 1355 M. K., Von Damm, K. L., & Voytek, M. A. (2006). A ubiquitous thermoacidophilic  
 1356 archaeon from deep-sea hydrothermal vents. *Nature*, *442*(7101), 444–447.  
 1357 <https://doi.org/10.1038/nature04921>
- 1358 Reysenbach, A.-L., Longnecker, K., & Kirshtein, J. (2000). Novel Bacterial and Archaeal  
 1359 Lineages from an In Situ Growth Chamber Deployed at a Mid-Atlantic Ridge  
 1360 Hydrothermal Vent. *Applied and Environmental Microbiology*, *66*(9), 3798–3806.  
 1361 <https://doi.org/10.1128/AEM.66.9.3798-3806.2000>
- 1362 Rinke, C., Rubino, F., Messer, L. F., Youssef, N., Parks, D. H., Chuvochina, M., Brown, M.,  
 1363 Jeffries, T., Tyson, G. W., Seymour, J. R., & Hugenholtz, P. (2019). A phylogenomic  
 1364 and ecological analysis of the globally abundant Marine Group II archaea (Ca.  
 1365 Poseidoniales ord. Nov.). *The ISME Journal*, *13*(3), 663–675.  
 1366 <https://doi.org/10.1038/s41396-018-0282-y>
- 1367 Rogers, D. R., Santelli, C. M., & Edwards, K. J. (2003). Geomicrobiology of deep-sea deposits:  
 1368 Estimating community diversity from low-temperature seafloor rocks and minerals.  
 1369 *Geobiology*, *1*(2), 109–117. <https://doi.org/10.1046/j.1472-4669.2003.00009.x>
- 1370 Rommevaux, C., Henri, P., Degboe, J., Chavagnac, V., Lesongeur, F., Godfroy, A., Boulart,  
 1371 C., Destrigneville, C., & Castillo, A. (2019). Prokaryote Communities at Active  
 1372 Chimney and *In Situ* Colonization Devices After a Magmatic Degassing Event (37°N  
 1373 MAR, EMSO-Azores Deep-Sea Observatory). *Geochemistry, Geophysics,*  
 1374 *Geosystems*, *20*(6), 3065–3089. <https://doi.org/10.1029/2018GC008107>
- 1375 Rosner, M., Ball, L., Peucker-Ehrenbrink, B., Blusztajn, J., Bach, W., & Erzinger, J. (2007). A  
 1376 Simplified, Accurate and Fast Method for Lithium Isotope Analysis of Rocks and  
 1377 Fluids, and  $\delta^7\text{Li}$  Values of Seawater and Rock Reference Materials. *Geostandards and*  
 1378 *Geoanalytical Research*, *31*(2), 77–88. <https://doi.org/10.1111/j.1751-908X.2007.00843.x>
- 1380 Ryu, J., Hong, J., Park, I.-S., Ryu, T., & Hong, H.-J. (2020). Recovery of strontium ( $\text{Sr}^{2+}$ )  
 1381 from seawater using a hierarchically structured  $\text{MnO}_2/\text{C}/\text{Fe}_3\text{O}_4$  magnetic  
 1382 nanocomposite. *Hydrometallurgy*, *191*, 105224.  
 1383 <https://doi.org/10.1016/j.hydromet.2019.105224>
- 1384 Santoro, A. E., Richter, R. A., & Dupont, C. L. (2019). Planktonic Marine Archaea. *Annual*  
 1385 *Review of Marine Science*, *11*(1), 131–158. <https://doi.org/10.1146/annurev-marine-121916-063141>
- 1387 Sarradin, P.-M., & Legrand, J. (2019). *MOMARSAT2019 cruise, RV Pourquoi pas?*  
 1388 <https://doi.org/10.17600/18001110>
- 1389 Schut, G. J., Lipscomb, G. L., Han, Y., Notey, J. S., Kelly, R. M., & Adams, M. M. W. (2014).  
 1390 The Order Thermococcales and the Family Thermococcaceae. In E. Rosenberg, E. F.  
 1391 DeLong, S. Lory, E. Stackebrandt, & F. Thompson (Eds.), *The Prokaryotes* (pp. 363–  
 1392 383). Springer Berlin Heidelberg. [https://doi.org/10.1007/978-3-642-38954-2\\_324](https://doi.org/10.1007/978-3-642-38954-2_324)
- 1393 Seyedali, M., Coogan, L. A., & Gillis, K. M. (2021). The effect of solution chemistry on  
 1394 elemental and isotopic fractionation of lithium during inorganic precipitation of calcite.  
 1395 *Geochimica et Cosmochimica Acta*, *311*, 102–118.  
 1396 <https://doi.org/10.1016/j.gca.2021.07.021>
- 1397 Sheik, C. S., Jain, S., & Dick, G. J. (2014). Metabolic flexibility of enigmatic SAR324 revealed  
 1398 through metagenomics and metatranscriptomics. *Environmental Microbiology*, *16*(1),  
 1399 304–317. <https://doi.org/10.1111/1462-2920.12165>
- 1400 Sievert, S. M., Kuever, J., & Muyzer, G. (2000). Identification of 16S Ribosomal DNA-  
 1401 Defined Bacterial Populations at a Shallow Submarine Hydrothermal Vent near Milos  
 1402 Island (Greece). *Applied and Environmental Microbiology*, *66*(7), 3102–3109.

- 1403 Slobodkina, G. B., Kolganova, T. V., Querellou, J., Bonch-Osmolovskaya, E. A., & Slobodkin,  
 1404 A. I. (2009). *Geoglobus acetivorans* sp. Nov., an iron(III)-reducing archaeon from a  
 1405 deep-sea hydrothermal vent. *INTERNATIONAL JOURNAL OF SYSTEMATIC AND*  
 1406 *EVOLUTIONARY MICROBIOLOGY*, 59(11), 2880–2883.  
 1407 <https://doi.org/10.1099/ijs.0.011080-0>
- 1408 Stahl, D. A. (1991). Development and application of nucleic acid probes in bacterial  
 1409 systematics. *Sequencing and Hybridization Techniques in Bacterial Systematics*.  
 1410 <https://cir.nii.ac.jp/crid/1571980075419733760>
- 1411 Swan, B. K., Martinez-Garcia, M., Preston, C. M., Sczyrba, A., Woyke, T., Lamy, D.,  
 1412 Reinthaler, T., Poulton, N. J., Masland, E. D. P., Gomez, M. L., Sieracki, M. E.,  
 1413 DeLong, E. F., Herndl, G. J., & Stepanauskas, R. (2011). Potential for  
 1414 Chemolithoautotrophy Among Ubiquitous Bacteria Lineages in the Dark Ocean.  
 1415 *Science*, 333(6047), 1296–1300. <https://doi.org/10.1126/science.1203690>
- 1416 Swartz, T. H., Ikewada, S., Ishikawa, O., Ito, M., & Krulwich, T. A. (2005). The Mrp system:  
 1417 A giant among monovalent cation/proton antiporters? *Extremophiles*, 9(5), 345–354.  
 1418 <https://doi.org/10.1007/s00792-005-0451-6>
- 1419 Takai, K., & Horikoshi, K. (2000). Rapid Detection and Quantification of Members of the  
 1420 Archaeal Community by Quantitative PCR Using Fluorogenic Probes. *Applied and*  
 1421 *Environmental Microbiology*, 66(11), 5066–5072.
- 1422 Takai, K., Oida, H., Suzuki, Y., Hirayama, H., Nakagawa, S., Nunoura, T., Inagaki, F.,  
 1423 Nealson, K. H., & Horikoshi, K. (2004). Spatial Distribution of Marine Crenarchaeota  
 1424 Group I in the Vicinity of Deep-Sea Hydrothermal Systems. *Applied and*  
 1425 *Environmental Microbiology*, 70(4), 2404–2413.  
 1426 <https://doi.org/10.1128/AEM.70.4.2404-2413.2004>
- 1427 Takai, K., Suzuki, M., Nakagawa, S., Miyazaki, M., Suzuki, Y., Inagaki, F., & Horikoshi, K.  
 1428 (2006). *Sulfurimonas paralvinellae* sp. Nov., a novel mesophilic, hydrogen- and sulfur-  
 1429 oxidizing chemolithoautotroph within the Epsilonproteobacteria isolated from a deep-  
 1430 sea hydrothermal vent polychaete nest, reclassification of *Thiomicrospira denitrificans*  
 1431 as *Sulfurimonas denitrificans* comb. Nov. And emended description of the genus  
 1432 *Sulfurimonas*. *International Journal of Systematic and Evolutionary Microbiology*,  
 1433 56(8), 1725–1733. <https://doi.org/10.1099/ijs.0.64255-0>
- 1434 Taylor, H. L., Duivesteyn, I. J. K., Farkas, J., Dietzel, M., & Dosseto, A. (2019). Technical  
 1435 note: Lithium isotopes in dolostone as a palaeo-environmental proxy – an experimental  
 1436 approach. *Climate of the Past*, 15(2), 635–646. <https://doi.org/10.5194/cp-15-635-2019>
- 1437 Teagle, D. A. H., Bickle, M. J., & Alt, J. C. (2003). Recharge flux to ocean-ridge black smoker  
 1438 systems: A geochemical estimate from ODP Hole 504B. *Earth and Planetary Science*  
 1439 *Letters*, 210(1–2), 81–89. [https://doi.org/10.1016/S0012-821X\(03\)00126-2](https://doi.org/10.1016/S0012-821X(03)00126-2)
- 1440 Teske, A., Hinrichs, K.-U., Edgcomb, V., de Vera Gomez, A., Kysela, D., Sylva, S. P., Sogin,  
 1441 M. L., & Jannasch, H. W. (2002). Microbial Diversity of Hydrothermal Sediments in  
 1442 the Guaymas Basin: Evidence for Anaerobic Methanotrophic Communities. *Applied*  
 1443 *and Environmental Microbiology*, 68(4), 1994–2007.  
 1444 <https://doi.org/10.1128/AEM.68.4.1994-2007.2002>
- 1445 Teske, A., Wegener, G., Chanton, J. P., White, D., MacGregor, B., Hoer, D., de Beer, D.,  
 1446 Zhuang, G., Saxton, M. A., Joye, S. B., Lizarralde, D., Soule, S. A., & Ruff, S. E.  
 1447 (2021). Microbial Communities Under Distinct Thermal and Geochemical Regimes in  
 1448 Axial and Off-Axis Sediments of Guaymas Basin. *Frontiers in Microbiology*, 12,  
 1449 633649. <https://doi.org/10.3389/fmicb.2021.633649>
- 1450 Thibon, F., Metian, M., Oberhänsli, F., Montanes, M., Vassileva, E., Orani, A. M., Telouk, P.,  
 1451 Swarzenski, P., & Vigier, N. (2021). Bioaccumulation of Lithium Isotopes in Mussel

- 1452 Soft Tissues and Implications for Coastal Environments. *ACS Earth and Space*  
1453 *Chemistry*, 5(6), 1407–1417. <https://doi.org/10.1021/acsearthspacechem.1c00045>
- 1454 Thibon, F., Weppe, L., Churlaud, C., Lacoue-Labarthe, T., Gasparini, S., Cherel, Y.,  
1455 Bustamante, P., & Vigier, N. (2023). Lithium isotopes in marine food webs: Effect of  
1456 ecological and environmental parameters. *Frontiers in Environmental Chemistry*, 3.  
1457 <https://www.frontiersin.org/articles/10.3389/fenvc.2022.1060651>
- 1458 Tomascak, P. B., Magna, T., & Dohmen, R. (2016). *Advances in Lithium Isotope*  
1459 *Geochemistry*. Springer International Publishing. [https://doi.org/10.1007/978-3-319-](https://doi.org/10.1007/978-3-319-01430-2)  
1460 01430-2
- 1461 Tor, J. M., & Lovley, D. R. (2001). Anaerobic degradation of aromatic compounds coupled to  
1462 Fe(III) reduction by *Ferroglobus placidus*. *Environmental Microbiology*, 3(4), 281–  
1463 287. <https://doi.org/10.1046/j.1462-2920.2001.00192.x>
- 1464 Vance, D., Teagle, D. A. H., & Foster, G. L. (2009). Variable Quaternary chemical weathering  
1465 fluxes and imbalances in marine geochemical budgets. *Nature*, 458(7237), 493–496.  
1466 <https://doi.org/10.1038/nature07828>
- 1467 Verney-Carron, A., Vigier, N., Millot, R., & Hardarson, B. S. (2015). Lithium isotopes in  
1468 hydrothermally altered basalts from Hengill (SW Iceland). *Earth and Planetary Science*  
1469 *Letters*, 411, 62–71. <https://doi.org/10.1016/j.epsl.2014.11.047>
- 1470 Vigier, N., Decarreau, A., Millot, R., Carignan, J., Petit, S., & France-Lanord, C. (2008).  
1471 Quantifying Li isotope fractionation during smectite formation and implications for the  
1472 Li cycle. *Geochimica et Cosmochimica Acta*, 72(3), 780–792.  
1473 <https://doi.org/10.1016/j.gca.2007.11.011>
- 1474 Vikström, H., Davidsson, S., & Höök, M. (2013). Lithium availability and future production  
1475 outlooks. *Applied Energy*, 110, 252–266.  
1476 <https://doi.org/10.1016/j.apenergy.2013.04.005>
- 1477 Von Damm, K. L., Bray, A. M., Buttermore, L. G., & Oosting, S. E. (1998). The geochemical  
1478 controls on vent fluids from the Lucky Strike vent field, Mid-Atlantic Ridge. *Earth and*  
1479 *Planetary Science Letters*, 160(3), 521–536. [https://doi.org/10.1016/S0012-](https://doi.org/10.1016/S0012-821X(98)00108-3)  
1480 821X(98)00108-3
- 1481 Voordeckers, J. W., Do, M. H., Hügler, M., Ko, V., Sievert, S. M., & Vetriani, C. (2008).  
1482 Culture dependent and independent analyses of 16S rRNA and ATP citrate lyase genes:  
1483 A comparison of microbial communities from different black smoker chimneys on the  
1484 Mid-Atlantic Ridge. *Extremophiles*, 12(5), 627–640. [https://doi.org/10.1007/s00792-](https://doi.org/10.1007/s00792-008-0167-5)  
1485 008-0167-5
- 1486 Waite, D. W., Vanwonterghem, I., Rinke, C., Parks, D. H., Zhang, Y., Takai, K., Sievert, S.  
1487 M., Simon, J., Campbell, B. J., Hanson, T. E., Woyke, T., Klotz, M. G., & Hugenholtz,  
1488 P. (2017). Comparative Genomic Analysis of the Class Epsilonproteobacteria and  
1489 Proposed Reclassification to Epsilonbacteraeota (phyl. Nov.). *Frontiers in*  
1490 *Microbiology*, 8. <https://www.frontiersin.org/articles/10.3389/fmicb.2017.00682>
- 1491 Waldron, K. J., & Robinson, N. J. (2009). How do bacterial cells ensure that metalloproteins  
1492 get the correct metal? *Nature Reviews Microbiology*, 7(1), 25–35.  
1493 <https://doi.org/10.1038/nrmicro2057>
- 1494 Wang, W., Jiang, S.-Y., & Xiao, Y. (2023). Fluid-rock interaction effects on Li isotope  
1495 behavior in continental geothermal systems. *Chemical Geology*, 631, 121525.  
1496 <https://doi.org/10.1016/j.chemgeo.2023.121525>
- 1497 Whitman, W., & Jeanthon, C. (2006). Methanococcales. In *The Prokaryotes: Vol. Vol. 3* (pp.  
1498 257–273). [https://doi.org/10.1007/0-387-30743-5\\_13](https://doi.org/10.1007/0-387-30743-5_13)
- 1499 Wissuwa, J., Bauer, S. L. M., Steen, I. H., & Stokke, R. (2017). Complete genome sequence of  
1500 *Lutibacter profundus* LP1T isolated from an Arctic deep-sea hydrothermal vent system.  
1501 *Standards in Genomic Sciences*, 12, 5. <https://doi.org/10.1186/s40793-016-0219-x>

- 1502 Wright, T. D., Vergin, K. L., Boyd, P. W., & Giovannoni, S. J. (1997). A Novel d-Subdivision  
1503 Proteobacterial Lineage from the Lower Ocean Surface Layer. *APPL. ENVIRON.*  
1504 *MICROBIOL.*, 63.
- 1505 Zeng, X., Alain, K., & Shao, Z. (2021). Microorganisms from deep-sea hydrothermal vents.  
1506 *Marine Life Science & Technology*, 3(2), 204–230. [https://doi.org/10.1007/s42995-](https://doi.org/10.1007/s42995-020-00086-4)  
1507 [020-00086-4](https://doi.org/10.1007/s42995-020-00086-4)
- 1508 Zhang, C. L., Xie, W., Martin-Cuadrado, A.-B., & Rodriguez-Valera, F. (2015). Marine Group  
1509 II Archaea, potentially important players in the global ocean carbon cycle. *Frontiers in*  
1510 *Microbiology*, 6.  
1511 <https://www.frontiersin.org/journals/microbiology/articles/10.3389/fmicb.2015.01108>
- 1512 Zhang, L., Kang, M., Xu, J., Xu, J., Shuai, Y., Zhou, X., Yang, Z., & Ma, K. (2016). Bacterial  
1513 and archaeal communities in the deep-sea sediments of inactive hydrothermal vents in  
1514 the Southwest India Ridge. *Scientific Reports*, 6, 25982.  
1515 <https://doi.org/10.1038/srep25982>
- 1516 Zillig, W., & Reysenbach, A.-L. (2015). Thermococci class. Nov. In *Bergey's Manual of*  
1517 *Systematics of Archaea and Bacteria* (pp. 1–1). John Wiley & Sons, Ltd.  
1518 <https://doi.org/10.1002/9781118960608.cbm00030>  
1519